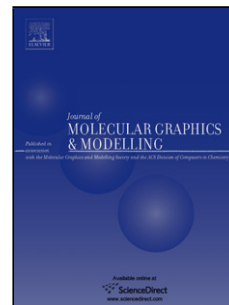# Accepted Manuscript

Title: The 3D-QSAR study of 110 diverse, dual binding, acetylcholinesterase inhibitors based on alignment independent descriptors (GRIND-2). The effects of conformation on predictive power and interpretability of the models

Authors: Maja D. Vitorović-Todorović, Ilija N. Cvijetić, Ivan O. Juranić, Branko J. Drakulić

Please cite this article as: M.D. Vitorović-Todorović, I.N. Cvijetić, I.O. Juranić, B.J. Drakulić, The 3D-QSAR study of 110 diverse, dual binding, acetylcholinesterase inhibitors based on alignment independent descriptors (GRIND-2). The effects of conformation on predictive power and interpretability of the models, *Journal of Molecular Graphics and Modelling* (2010), doi:10.1016/j.jmgm.2012.08.001

Highlights:

►3D QSAR study on the set of 110 diverse dual binding AChE inhibitors is reported.
► Three types of conformations were used for derivation of the models.
► The most important variables were expressed in all three models.
► Protonated pyridinium nitrogen was proved as highly important for inhibition potency.
► Structurally diverse, external set (40 compounds) is well predicted by the models.
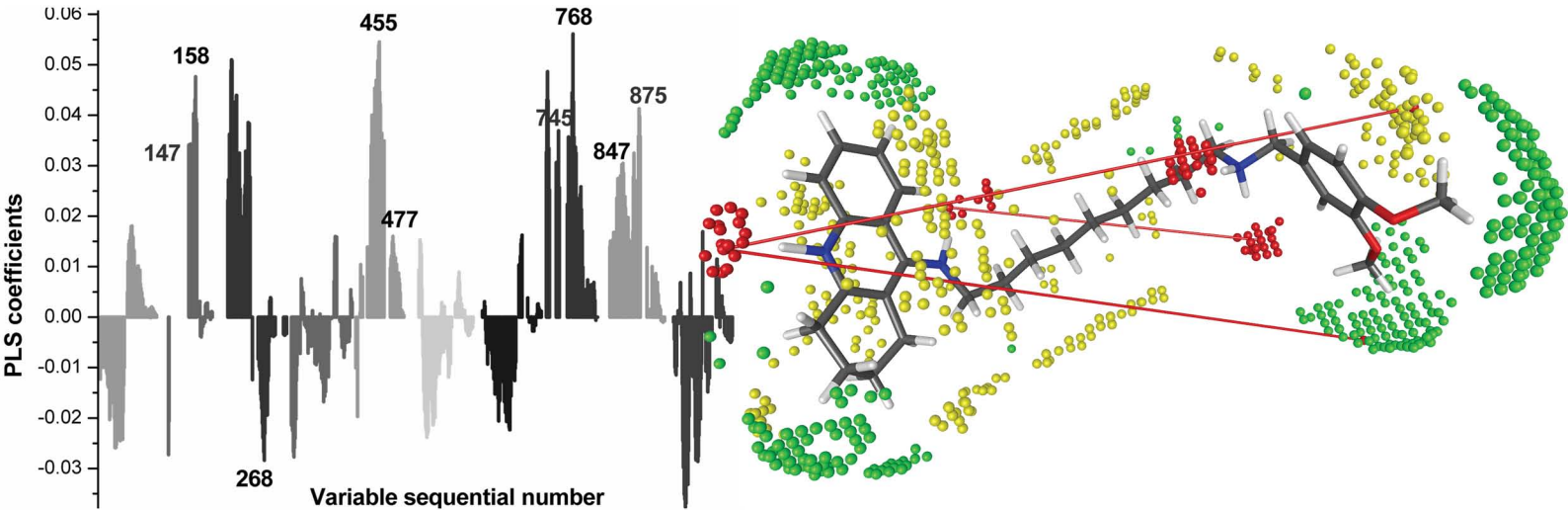
The 3D-QSAR study of 110 diverse, dual binding, acetylcholinesterase inhibitors based on alignment independent descriptors (GRIND-2). The effects of conformation on predictive power and interpretability of the models

Maja D. Vitorović-Todorović,[1,2,*] Ilija N. Cvijetić,[2] Ivan O. Juranić,[3] and Branko J. Drakulić[3]

[1] *Military-Technical Institute, Ratka Resanovića 1, Belgrade, Serbia*

[2] *Faculty of Chemistry, University of Belgrade, Studentski trg 12-16, Belgrade, Serbia*

[3] *Department of Chemistry-IChTM, University of Belgrade, Njegoševa 12, Belgrade, Serbia*

---

[*] Correspondence to: Maja Vitorović-Todorović, Tel.: +381 11 3336738; fax: +381 11 2636061
(E-mail: mvitod@chem.bg.ac.rs)

1

Abstract

The 3D-QSAR analysis based on alignment independent descriptors (GRIND-2) was performed on the set of 110 structurally diverse, dual binding AChE reversible inhibitors. Three separate models were built, based on different conformations, generated following next criteria: (*i*) minimum energy conformations, (*ii*) conformation most similar to the co-crystallized ligand conformation, and (*iii*) docked conformation. We found that regardless on conformation used, all the three models had good statistic and predictivity. The models revealed the importance of protonated pyridine nitrogen of tacrine moiety for anti AChE activity, and recognized HBA and HBD interactions as highly important for the potency. This was revealed by the variables associated with protonated pyridinum nitrogen, and the two amino groups of the linker. MIF's calculated with the N1= (pyridinium nitrogen) and the DRY GRID probes in the AChE active site enabled us to establish the relationship between aminoacid residues within AChE active site and the variables having high impact on models. External predictive power of the models was tested on the set of 40 AChE reversible inhibitors, most of them structurally different from the training set. Some of those compounds were tested on the different enzyme source. We found that external predictivity was highly sensitive on conformations used. Model based on docked conformations had superior predictive ability, emphasizing the need for the employment of conformations built by taking into account geometrical restrictions of AChE active site gorge.

Key words: Acetylcholinesterase; dual binding inhibitors; GRIND-2; 3D-QSAR; molecular interaction fields, external predictivity

2

1. Introduction

Alzheimer's disease (AD) is progressive, neurodegenerative disorder, characterized by the decrease of cognitive functions such as altered ability of memory and learning and behavioural disturbances. The main pathological hallmarks of the disease comprise: extracellular formation of senile amyloid-β-peptide (Ab) plaques [1], intracellular formation of neurofibrillary tangles [2,3], the loss of cholinergic neurons from basal forebrain, and thereby decreased levels of neurotransmitter acetylcholine (ACh) and enzymes involved in its synthesis and hydrolysis: acetylcholinetransferase (ChAT) and acetylcholinesterase (AChE) [4,5]. Development of new therapeutics for AD is based on two different strategies, the so-called cholinergic and the amyloid hypothesis. According to the cholinergic hypothesis, the increase in available ACh levels in the brain could induce cognitive improvements in AD patients. The reduction of ACh hydrolysis by AChE inhibitors is up to date the prevalent effective AD symptomatic treatment. On the other hand, amyloid hypothesis suggest that amyloid polymerization (aggregation) could play crucial role in neurodegenerative process by disrupting the cell's calcium homeostasis, inducing the oxidative stress, and consequently neuronal apoptosis [6]. The formation of senile plaques involves cascade of events, most important of them being cleavage of transmembrane amyloid precursor protein (APP) by β- or γ-secretase, *i.e.* generation of soluble amyloid-beta peptides. These soluble peptides can spontaneously form larger aggregates. This leads to formation of insoluble senile plaques [7,8]. The development of drugs based on amyloid hypothesis involves β- or γ-secretase inhibitors.

AChE contains 20 Å deep and narrow gorge, in which five regions involved in the substrate and inhibitor binding can be distinguished (*Torpedo Californica* AChE numbering): (1) catalytic triad residues: Ser 200, His 440, and Glu 327 [9], at the bottom of the gorge, which directly

3

participate in catalytic cycle [10,11]; (2) oxyanion hole - stabilizes the transient tetrahedral enzyme–substrate complex by accommodation of negatively charged carbonyl oxygen of acetylcholine. This region is formed by backbone –NH– groups of amino acid residues Gly 118, Gly 119, and Ala 201 [12,13]; (3) the 'anionic site' (AS), where Trp 84 is situated. This residue is conserved in all cholinesterases and is involved in orientation and stabilization of trimethylammonium group of ACh, by forming cation–π interactions [14-16]; (4) acyl pocket, comprises two phenylalanine residues in positions 288 and 290, that interact with the substrate acyl group [17]; (5) peripheral anionic site (PAS) [18-20] comprises residues located at the rim of the active site gorge, Tyr 70, Tyr 121, Trp 279, and Asp 72. Reversible inhibitors bind to AS or to PAS. The so-called dimeric (dual) inhibitors bind simultaneously to both of the sites. In the past decade, non-catalytic roles of AChE have been established. It was proved that AChE has a key role in the acceleration of Aβ-peptide deposition, promoting the formation of Aβ-plaques [21]. The dual-binding AChE inhibitors, which bind to PAS, could inhibit such processes [22]. Dual AChE inhibitors represent the important class of molecules, because they fill the gap between holinergic and amyloid hypothesis, combining the two biological activities in single molecular entity.

Correlation of pharmacological property (biological activity) with 3D description of drug molecule, and hereby identification of drug features that contribute to its potency, represents the central problem in the field of drug design. Numerous methods for 3D QSAR analysis have been developed from the early 80's of the last century, with the CoMFA [23] being the most widely used technique. So, it is not surprising that CoMFA and related methods (CoMSIA) were widely employed in modelling of AChE inhibitors. CoMFA is applied to a series of compounds that are aligned according to the specified criterion in 3D space. Next, the aligned molecules are described by different 3D fields (originally only steric and electrostatic fields were used), evaluated over a

4

grid of points, using suitable probe type. Partial least square analysis (PLS) is used for correlation of the CoMFA derived descriptors with the biological activity.

Alignment of the molecules is the most crucial point in performing successful CoMFA study, and represents a bottleneck and major source of errors in CoMFA analysis. However, there are no strict rules for the alignment. If structural data about target-ligand complexes are not available, molecules are aligned using all the other available information, pharmacophoric hypothesis, similar molecular fragments, etc. For instance, Tong and co-workers [24] performed a CoMFA study on the set of 57 structurally similar *N*-benzylpiperidinyl AChE inhibitors. Two types of alignment were used to optimize steric or electrostatic fitting between molecules. The later alignment method gave statistically better model. Also, common substructure fitting [25], pharmacophore based [26], and atom based alignment (implemented in SYBYL) [27] were used as alignment protocols for derivation of CoMFA models for AChE inhibitors.

If a structure of biological target is known, then techniques of the so-called structure based alignment could be used, which involve conformer-based alignment using co-crystalized ligand as the template, and docking based alignment. Recanatini and co-workers [28] docked two representative molecules into AChE active site and used the obtained complexes for superimposition of the rest of molecules for the alignment. Statistically highly significant CoMFA model was obtained, using a steric field alone. Chen and co-workers [29] compared ligand based alignment and docking based alignment, obtained by AutoDock, in derivation of CoMFA/CoMSIA models for the set containing 60 tacrine-dihydopyridine hybrids. All models obtained gave good statistics and predictivity, but the authors considered docking based model as more reliable. Also, GOLD program was used for docking based alignment in CoMFA/CoMSIA study of 36 2-substituted aminoindanones [30]. Structure of AChE cocrystalized with gantstigmine was used as

5

alignment template for 40 physostigmine derivatives [31]. This strategy yielded statistically significant CoMFA/CoMSIA models.

Research efforts have also been made in the development of alignment independent descriptors. Those are CoMMA [32], EVA [33], and WHIM [34]; with EVA descriptors being the least sensitive to conformation of compounds. Recently, Pastor and co-workers [35] developed the alignment independent, so-called GRid INDependent (GRIND) descriptors. Instead of using field values for PLS analysis, the pair of nodes (GRID MIF minima) calculated by the four GRID probes, are used as descriptors (variables). Only those pairs of nodes (for the same, or for different probe type) that have the highest product of interaction energy (IE), at the given distance range, are used for PLS analysis. This method, although alignment independent, and according to the authors robust on small to medium conformational changes, requires that the conformation used should be the best assessment of bioactive conformation. Such conformations could be significantly different from the global minimum conformation, obtained in vacuum or in solvent model.

We decided to apply the last described method on the set of 110 AChE dual binding inhibitors, and to investigate how conformations chosen by different reasoning, will influence the statistics and interpretability of the models. Dual binding inhibitors represent a good choice for such analysis. They comprise two aromatic cores linked by polymethylene chain. They are highly flexible and theoretically could adopt different conformations even inside AChE gorge. An additional benefit of the alignment independent descriptors is that training set could comprise structurally very different compounds. To the best of our knowledge, the set given in this study is one of the largest, and chemically the most diverse set used for 3D-QSAR analysis of AChE inhibitors. There is a lot of crystallographic data on AChE-ligand complexes, so we were able to compare the obtained results with the most common interactions that can be found in AChE-ligand

6

complexes. Predictivity of the models was tested by the division of the original set on the training and test set, and also by the external test set comprising 40 molecules, structurally diverse comparing to the original set of 110 AChE inhibitors.

2. Methods

2.1 Description of the dataset

Six groups of structurally different compounds were used, including: *N*-benzylpiperidine derivatives (**1-11**) [36], homodimeric quinazolinimines (**12-32**) [37], heterodimers of quinazolinimine and lipoic acid (**33-38**) [38], bis-pyridinum type inhibitors (**40-67**) [39,40], heterodimers of tacrine and substituted benzene derivatives (**39**, **68-80** and **97-110**) [41,42,43], and tacrine-xanomeline dimmers (**81-96**) [44], yielding totally 110 compounds in the dataset, with activity range of four $p(IC_{50})$ units. Because experimental data were collected from the different research groups, the experimental conditions for IC_{50} determination against AChE were carefully examined and compared. All experiments were done using the same, Ellman spectrophotometric assay [45], at pH 8.00, with ASCh as substrate. The Electic Eel AChE was used as enzyme source. IC_{50} values for tacrine, as reference compound, were comparable in all series of compounds; except for the set of tacrine-substituted benzene heterodimers. The measured tacrine potency in this experiment was about four times lower. So, we renormalized IC_{50} values for this group of compounds, using IC_{50} values obtained for tacrine, according to the recommendation of Martin-Santamaria *et al.* [46].

7

2.2 Conformations of the molecules

Conformations were chosen based on different criteria, and the three separate models were built. (i) SMILES notations of all compounds used in model were converted to 3D by OMEGA [47], using MMFF94s [48] force field (build and search). Up to two hundred conformations per compound were generated. Conformation of each compound with the lowest heat of formation was used for building of the first model. In the rest of the text, we designate this model as 'OMEGA model';

(ii) Conformations for the second model were obtained using crystal structure of the AChE complexed with *bis*(7)tacrine inhibitor as a template, PDB code 2CKM. The coordinates of the inhibitor were extracted from the PDB file and used as template for superimposition by ROCS [49] program. Conformers generated by OMEGA in the first step, were submitted to ROCS program, and conformation of each compound most similar to the conformation of *bis*(7)tacrine were chosen for the building of the second model. In the ROCS program hits were ranked by default Tanimoto function. Under the shape options, the 'shape only', and 10 random starts are chosen. The Tanimoto cut-off is set to −1. In the rest of the text, we designate this model as 'ROCS model';

(iii) For the third model, conformations were generated by docking of compounds to AChE crystal structure, PDB code 2CKM, by AutoDock Vina 1.0 [50]. The all water molecules found in the crystal structure were included. In the rest of the text, we designate this model as 'VINA model'. The box that include both AS and PAS residues is defined manually in MGLTools (box size 26 x 28 x 20 Å). Grid resolution is set to 1 Å, as default in Vina, 'exhaustiveness' is set to 20, and energy range to 4. Docked pose of the native ligand almost ideally reproduced cocrystallized one. For the model building we chose the poses that are not necessary 'best ranked' ones obtained by docking. For the tacrine comprising molecules, the first pose having tacrine moiety in the AS is

8

chosen. If the best ranked pose represents bent conformation (as found for molecules having long linkers), we chose the next pose representing the extended conformation. All conformations included in the model are within the first three best ranked ones, as obtained by docking. All calculations by ROCS and AutoDock Vina were run on a multi-node Linux based cluster equipped with 2 x quad core Intel Xeon-E5345 @ 2.33 GHz processors, in parallel or sequential mode.

2.3 Calculating descriptors and model building

Models were built using Pentacle program. Protonation state of each compound was ascribed by the program under pH 8.0, as reported in the original reference. Pentacle uses AMANDA [51] algorithm to produce the second generation of alignment-independent molecular descriptors (GRIND-2). Descriptors are obtained from GRID [52] molecular interaction fields (MIFs). Derived GRID MIF minima are encoded in the variables that describe pair of nodes (interaction energy (IE) of each node and the corresponding distance between nodes); descriptors are further processed by means of built-in PCA/PLS (principal component analysis/partial least squares) statistical tool. For the model generation N1, O, TIP and DRY probes were used, with GRID resolution of 0.4 Å. For the encoding, maximum auto and cross-correlation (MACC2) algorithm were applied. Probes cut-off was hold on default value, as well as MACC2 smoothing window and scale factor. Validation of the models was done by cross-validation using five groups of the approximately same size in which the objects were assigned randomly. For the final models, the leave two out, and the leave one out cross-validation data are also reported.

2.4. Predictivity of the models

Predictivity of the models was tested by random division of the original set on the training and the test set (comprising 32 compounds, designated as 'test set1'). Predictivity was further tested by

9

truly external test set of the compounds, most of them structurally dissimilar from the compounds in the original training set and some of them tested on different enzyme source (designated as 'test set 2'). For this test set, we collected totally 40 compounds, comprising: 2,4-disupstituted pyrimidines (**111-119**, structurally dissimilar and tested on *Hu*AChE) [53], dual tacrine congeners (**121-123**, structurally similar, but tested on *Hu*AChE) [54], piperidine derivatives (**124-134**, structurally dissimilar and tested on *Ee*AChE) [55], indanone derivatives (**135-145**, structurally dissimilar and tested on *Ee*AChE) [56] and tacrine-ferulic acid dimers (**145-150**, structurally similar and tested on *Ee*AChE) [57]. Conformations of the compounds were generated in the same way as for the training set, using OMEGA program for generating conformations, ROCS for choosing the most similar conformation to co-crystalized ligand, and AutoDock Vina program for docking. Where necessary, IC_{50} values were renormalized according to the value for tacrine, in the same way as for the training set. Predictivity was expressed in terms of r^2 predictive values, for both test set 1, and test set 2.

3. Results and discussion

The aim of this study was to derive 3D-QSAR models, based on the alignment independent descriptors (GRIND-2) for the set of 110 AChE dual-binding inhibitors. Dual binding AChE inhibitors are composed of two aromatic cores connected with polymethylene chain and therefore are highly flexible. As we mentioned above, although applied method is insensitive on small to medium conformational changes, employment of conformations most similar to the approximated bioactive conformation is recommended. We have built three separate models, with different conformations obtained following next criteria: global minimum conformation, maximum similarity with co-crystallized ligand, and docked conformations. We aimed to investigate how conformational differences will influence the final models. The structures of compounds and their

10

experimental pIC_{50} are shown in Schemes 1 and 2, and Table 1. For the model building, hydrophobic (DRY), hydrogen bond donor, HBA (O), hydrogen bond acceptor, HBD (N1), and shape (TIP) probes were used. These probes mimic the most common types of interactions between ligand and receptor. The models obtained had good statistic and predictivity (Table 2.). The model derived from ROCS conformations showed the best statistical quality. Data of PCA models, and experimental *vs*. calculated pIC_{50} are given in Supplementary material, Tables S1and S2. Partial least squares (PLS) coefficient plots obtained with 3 latent variables (LV) for the each model are shown in Figure 1.

Please put the Scheme 1 here

Please put the Scheme 2 here

The main observations, that give significant information on the pharmacophoric pattern of the molecules influencing their potency, will be discussed for the each model separately. Two groups of compounds comprise tacrine subunit (Scheme 2). The obtained results are interpreted according to the widespread assumption, based on the large amount of crystallographic and SAR data, that tacrine subunit binds to AS of AChE. This was also in accordance with the docking poses obtained for the majority of **1-110**.

Please put the Table 1 here

Please put the Table 2 here

Please put the Figure 1 here

11

3.1 Description of the conformations

The detailed description of derived docking poses for all compounds is beyond the scope of this article, but a few important points should be mentioned. All compounds containing tacrine moiety are positioned inside AChE active site with the tacrine stacked between aromatic rings of Trp 84 and Phe 330 (AS residues), and the "upper" aromatic (tacrine-benzene dimers, **68**-**80** and **97**-**102**) or alicyclic piperidine (tacrine-xanomeline dimers, **81**-**96**) moiety is stacked between aromatic rings of Trp 279 and Tyr 70. We have also observed that bispyridinium compounds (**40**-**59**) are bound with the one aromatic ring interacting with AS residues, but as compounds are very long, they are unable to establish the interactions with Trp 279 and Tyr 70 of the PAS; so the "upper" aromatic ring protrudes outside the AChE gorge and does not establish any significant interactions with AChE residues.

Dimeric quinazolinimines were oriented similarly to the tacrine-containing compounds. For the quinazolinimine-lipoic acid heterodimers, docking results showed more poses with lipoic acid, comparing to qiunazolinimine moiety, interacting with the Trp84. This emphasizes the lower affinity of quinazolinimine aromatic core to anionic site of the enzyme. Important docking poses are given in Figure S3, Supplementary material.

3.2 Model based on OMEGA conformations of minimal energy

The most important variables for this model are shown in Figure 2. The expression of the important variables for all compounds is given in Supplementary material, Table S4.

In the O-O block, all variables positively correlated with activity have high impact on the model and are expressed only for the most active compounds. Variable O-O 147 (14.08-14.40 Å)

12

connects: the MIFs' associated with two linker amino groups, in extended conformations of tacrine-benzene dimmers, or protonated pyridine nitrogen of tacrine subunit and distal amino group of the linker in bent conformations of tacrine-xanomeline and tacrine-benzene dimers. Variables O-O 150 (15.04-15.36 Å), 156 (16.96-17.28 Å), and 158 (17.60-17.92) connect MIF's associated with pyridine nitrogen of the tacrine subunit and distal linker amino group of tacrine-benzene dimers. Clearly, the presence of two hydrogen bond donors of molecules, associated with MIFs, on the spatial distance from 14.08 to 17.28 Å, has positive influence on the potency, and distinguishes the most active compounds from the rest in the series.

In N1-N1 block, the most informative variables are those with the negative impact on the model. Variables 263 (18.24-18.56 Å), 267 (19.52-19.84 Å), and 268 (19.84-20.16 Å) connect the MIFs' associated with two distal oxygen atoms of bis-pyridinium derivatives or two distal heterocyclic nitrogen atoms of homodimeric quinazolimines. They are expressed only for the less active compounds. The presence of two hydrogen bond acceptors, associated with MIFs', on the spatial distance greater than 18.88 Å has negative effect on AChE inhibition potency, and makes the clear distinction between the least active compounds and the rest of the molecules.

In DRY-O block, variable 455 (13.76-14.08 Å) has high positive impact on the model and is expressed for all active compounds (Supplementary material, Table S4). For majority of tacrine-benzene dimers, this variable connects MIFs' associated with the hydrophobic area of tacrine aromatic ring and with the distal amino group of the linker. These compounds adopted extended conformations. Similarly, the same variable connects MIFs' associated with DRY area of quinazolinimine ring and with the distal amino group of the linker (compounds **12-38**). For the tacrine-xanomeline dimers, the interpretation of this variable is not straightforward, because of the bent conformations of molecules. The variable connects MIFs' associated with protonated pyridine

13

nitrogen (HBD) and either hydrophobic area of the xanomeline tetrahydropyridine ring, or hydrophobic area in the middle of the linker. For some compounds, the same variable connects DRY area on xanomeline dehydropyridine ring and the HBA area on amino group of the linker. Variable 463 (16.32-16-64 Å) describes the same pharmacophoric pattern. Variable 477 (20.80-21.12) has the lower impact on the model, but it differentiates the most active tacrine-benzene dimers from the rest of the compounds. It connects MIFs' associated with protonated pyridinium nitrogen (HBD) and hydrophobic area above the benzene ring; or the hydrophobic area above tacrine moiety and –OH substituent at the benzene ring. So, the presence of hydrophobic moiety and hydrogen bond donor on the spatial distance of about 20 Å is an attribute of the most active compounds.

Although expressed for the vast majority of compounds, variable 745 (7.68-8.00 Å) in the O-N1 block, could be informative for the pharmacophoric pattern favourable for PAS binding. It connects MIFs' associated with the distal amino group of the linker and alkoxy substituent on the benzene ring of the tacrine-benzene dimers. Giving the assumption that tacrine moiety binds to AS (Trp 84), and benzene moiety interacts with PAS (Trp 279 and proximal amino acids), this variable could provide information about favourable structural elements for binding to the PAS. For the tacrine-xanomeline dimmers, this variable cannot be interpreted in the same way. Most of these compounds are present in bent conformations, having two aromatic moieties close to each other. For those molecules, variable 745 connects two structural moieties which are spatially close in conformations used, but probably distant in bioactive (bound) conformation. Variable O-N1 768 (15.04-15.36 Å) has the most positive impact on the model, and connects MIFs' associated with alkoxy group of tacrine-benzene dimmers and proximal amino group of the linker; or pyridinium nitrogen of the tacrine moiety and amide carbonyl group of the linker in tacrine-xanomeline

14

dimmers. The same variable connects quinazolinimine nitrogen atom (N1) with distal amino group of the linker in homodimeric quinazolinimines. Similar structural elements are described by longer variables within this block. Those variables are expressed for the more active compounds.

In O-TIP block variable 849 (8.00-8.32) provides information about structural elements favourable for binding both to AS and to PAS of the enzyme. In tacrine-xanomeline dimmers it connects MIFs' associated with pyridinium nitrogen (O) and with the aromatic ring of tacrine (TIP), as elements favourable for AS binding. In tacrine-benzene dimmers the same variable connects MIFs' associated with amino group of the linker (O), and with the alkoxy groups on the benzene ring (TIP). Variable O-TIP 876 (16.64-16.96 Å), has the most positive impact within this block, and describes pharmacophoric pattern that is favourable for simultaneous binding to AS and PAS. It connects aromatic ring of tacrine (TIP) or quinazolineimine moiety, and distal amino group of the linker (O) in tacrine-benzene dimers or homodimeric quinazolinimines.

Please put the Figure 2 here

3.3 Model based on ROCS derived conformations

The most important variables for this model are shown in Figure 3. The expression of the important variables for all compounds is given in Supplementary material, Table S5.

In O-O block, variable 128 has the highest negative impact on the overall model. It describes MIFs' associated with two hydrogen bond donors on the spatial distance from 6.40 to 6.72 Å, and connects structurally different elements, even for the compounds within the same subset. For some compounds, same variable connects MIFs' associated with two amino groups of the polymethylene linker, feature that is usually considered beneficial for anti-AChE activity [58].

15

Variables O-O 144 (11.52-11.84 Å) and 161 (16.96-17.28 Å) provide the same type of information as variables 143, 150, 156, and 158 in OMEGA model, although distances are slightly different.

In the N1-N1 block, variable 234 (5.76-6.08 Å) has the most positive impact within the block, although it is not expressed for the most active compounds in the dataset. This variable could offer the information on favourable pharmacophoric pattern for binding to the PAS. In the tacrine-xanomeline dimers, it connects MIFs' associated with nitrogen of thiadiazoline ring and with the tetrahydropyridine nitrogen, or with the amide nitrogen. In the tacrine-benzene dimers variable connects MIFs' associated with the two alkoxy oxygens on the benzene ring. Therefore, the presence of two hydrogen bond acceptors at spatial distance 5.76 to 6.08 Å could be considered as favourable for binding to the PAS. Variable is expressed only in the ROCS model. Variables 278 (19.84-20.16 Å) and 280 (20.48-20.80 Å) are comparable with the variables 263-268 in OMEGA model.

Variable DRY-O 475 (13.76-14.08 Å) provides the same information as variable 455 in OMEGA model. Also, it has the most positive impact within this block. This variable describes slightly different structural fragments of tacrine-xanomeline dimers, comparing to OMEGA model, since these compounds are present in more extended conformations in ROCS model. It connects DRY area related to xanomeline fragment with the O field, associated with either protonated pyridinium nitrogen or distal amino group of the linker, depending on the linker length, and on conformation of the particular compound. Variable DRY-O 496 (20.48-20.80 Å) nicely differentiates the most active compounds from the rest of the set, and is comparable to variable 477 in the OMEGA model. Variable O-N1 805 (15.68-16.00 Å) has the highest positive impact on the model, and along with the related variables (803 and 806) provides the same information as the variable 768 in OMEGA model.

16

In O-TIP block, variable 888 (7.68-8.00 Å) provides the same type of information as variable 849 in OMEGA model, about structural elements favourable for simultaneous binding to AS and PAS of the enzyme. Variable O-TIP 930 (21.12-21.44 Å) is expressed only for the most active compounds in the dataset and connects MIFs' associated with pyridine nitrogen of tacrine subunit and with the most distal part of dual tacrine-xanomeline or tacrine-benzene heterodimers.

Please put the Figure 3 here

3.4 Model based on VINA docked conformations

The most important variables for this model are shown in Figure 4. The expression of the variables for all compounds is given in Supplementary material, Table S6.

Variable DRY-DRY 66 (21.12-21.44 Å) has moderate negative impact on the model, and is expressed only for the less potent compounds. Variable connect MIFs' associated with the two distal benzyl groups of pyridinium dimers. In dual AChE inhibitors, the one aromatic group interact with AS (Trp 84), the chain spanning along the active site gorge, and the other aromatic moiety interacts with PAS (Trp 286). The influence of linker length on AChE inhibition potency is well documented in the literature [59]. So, this variable shows that too long linker in the dual binding inhibitors cause decrease in inhibition potency, because of the lack of proper positioning of aromatic moiety in the PAS, and its interaction with Trp 279.

The variable 123 (8.64-8.96 Å) has high positive impact in the O-O block. In the different subsets, this variable describes structurally different elements of the compounds. Variable connects MIFs' associated with the protonated pyridinium nitrogen and with the amino group of linker close to tacrine moiety, in tacrine-xanomeline dimmers; or MIFs' associated with the two amino groups

17

of the linker in tacrine-benzene dimers, and in quinazolinimine heterodimers. The O-O variable 135 (12.48-12.80 Å), resembles variables 143 in OMEGA, and 147 in ROCS model, and has very low impact on the model. Variable 147 (16.32-16.64 Å) connects MIFs' associated with the protonated pyridinium nitrogen and the distal linker amino group of tacrine-benzene dimers. It resembles variable 158 in the OMEGA model, and variable 161 in the ROCS model.

The N1-N1 block provides similar type of information as in other two models; variable 241 (15.68-16.00 Å) gives the same type of information as somewhat longer variables (> 18.00 Å) in other two models. In DRY-O block, variable 427 (13.76-14.08 Å) provides the same information as variables 455 and 475 in other two models. The same is true for variable 444 (19.20-19.52 Å), and variables 477 and 496 in OMEGA and ROCS models, respectively.

In O-N1 block, variables 697 (8.00-8.32 Å) and 698 (8.32-8.64 Å) have moderate negative impact on the whole model. These variables depict the same pharmacophoric pattern as variable 745 in OMEGA model, positively correlated with the potency. Variables connect MIFs' associated with the distal amino group of the linker, and with the alkoxy substituents on the benzene ring in tacrine-benzene dimers. Such pharmacophoric pattern is perceived as favourable for binding to PAS in OMEGA model, but as unfavourable in the model derived by using the docked conformations. Variable O-N1 723 (16.32-16.64 Å) has the overall highest positive impact on the model, and provides the comparable information as variables 768 and 805 in OMEGA and ROCS model, respectively.

The variable O-TIP 791 (7.36-7.68 Å) describes the same structural fragments of compounds as variables 849 and 888 in OMEGA and ROCS model, respectively; but it has very low positive impact on the model derived from docked conformations. Variable 832 (20.48-20.80

18

Å) provides the same information as variable 930 in ROCS model, and is expressed only for the most active compounds in the set.

Please put the Figure 4 here

Please put the Table 3 here

The most important variables, their expression, and the related structural elements of compounds are shown in Table 3. Regardless of conformation, all three models have good statistics and predictivity. Comparative analysis, as presented in Table 3, shows that the most important variables are expressed in all three models. Structural elements of the compounds that have favourable influence on anti-acetylcholinesterase potency are:

- Protonated pyridinium nitrogen (of the tacrine subunit) and distal linker amino group; or the two amino groups of the linker, at a distance greater than 14 Å, as described by long O-O variables.

- Protonated pyridinium nitrogen (O) and distal DRY area (xanomeline or benzene moieties), which probably interacts with PAS residues, described by variables 477, 496, and 444 in OMEGA, ROCS, and VINA models respectively.

- Proximal amino group (O) of the linker and alkoxy substituents on the benzene ring, or imino group of quinazolineimine ring (N1), described by variables 768, 805 and 723 in OMEGA, ROCS, and VINA models, respectively. These variables have the highest positive impact in all models.

- Protonated pyridinium nitrogen (O) and endmost part of the molecules (TIP), as described by variables 876, 930, and 832 in OMEGA, ROCS, and VINA models, respectively.

19

Everything so far described emphasizes the importance of protonated pyridinium nitrogen for AChE inhibition activity. According to the crystal structures of AChE co-crystalized with the tacrine and tacrine-related dual inhibitors, protonated pyridinium nitrogen forms hydrogen bond with backbone carbonyl group of His 440, the residue of the catalytic triad [60]. Dual quinazolinimine-containing compounds (**12-32**) have structural elements favourable for anti AChE activity, similar to the tacrine based inhibitors. This is revealed by the intensive DRY-O and O-TIP variables (455 and 875, OMEGA model), expressed for the both subset of compounds. Heterocyclic nitrogen of quinazolinimine containing compounds has the higher pK_a value, comparing to tacrine nitrogen, and consequently is not protonated at assay pH. Therefore, the variables important for AChE activity, O-O 158 and DRY-O 477, which connect MIF's associated with protonated heterocyclic nitrogen with other structural elements of tacrine-based compounds, are not expressed for quinazolinimine containing compounds. Providing the importance of such observation for the interpretation of the models, we estimated protonation sates by independent software, ADMET Predictor (Simulations Plus, Inc.) [61], for the two representative compounds, that belong to dual quinazolinimines (compound **16**), and to tacrine benzene dimers (compound **107**). The results obtained were in accordance with protonation states ascribed by Pentacle. Predominant microstates, on the experimental conditions (pH 8.00), show the protonated heterocyclic nitrogen of tacrine moiety in compound **107**, while the 'pyridinium' nitrogen of quinazolineimine in compound **16** is not protonated**,** see Table S7 and Figures S8 and S9 in Supplementary material. Therefore, the lack of the protonation of heterocyclic nitrogen could be considered as the main reason for the lower potency of quinazolinimine dimers.

The most important structural element of the compounds, having negative impact on anti-AChE activity, in all three models, is the presence of MIFs', at spatial distance greater than 18 Å,

20

associated with two HBA. Such structural elements are two oxime oxygens of bispyridinium compounds, and two unprotonated heterocyclic nitrogens of homodimeric quinazolinimines.

The major differences between three models we found for the short variables (< 8.00 Å). We have tried to identify short variables that can describe specific structural elements favourable for binding to the AS or to the PAS of the AChE. Such variables are identified in the three blocks, N1-N1, O-N1 and O-TIP (Table 2.), but they were not expressed in all models, or did not have the same impact on the models. We have built separate models only for tacrine-related dual inhibitors (**68-110**) (results not shown) in order to find variables that describe favourable structural elements for binding to PAS. Although we obtained statistically relevant models, short variables had even lower intensities in PLS models than in the original model. Generally, we had the problem with interpretation of short variables, because they were related to different structural elements of the compounds, even within the same subset. This is especially evident in the N1-N1 block, for all three models reported. Short variables have high positive impact on the models, but the important common structural features relevant for high potency cannot be anticipated. Considering the fact that short variables have different influence (positive or negative), and impact (high or low) in different models, we are able to conclude that they are less interpretable in describing structure-activity relationships.

The other difference between three models lies in different expression pattern for DRY-DRY variables (see PLS coefficients plots, Figure 1). In OMEGA model the short variables are negatively correlated with potency, and longer variables are positively correlated with potency. In model based on VINA docked conformations we found reverse situation. In ROCS model all DRY-DRY variables were positively correlated with potency. So far we cannot offer explanation for this. It is also unusual that all three models recognized HBD and HBA interactions as the most

21

important for the potency of compounds, even more important then hydrophobic interactions, as revealed by intensities of variables in the O-O and O-N1 blocks. We did not expect such result, considering the fact that AChE active site gorge is lined with 14 aromatic aminoacid side chains. The importance of hydrophobic interactions could be anticipated only from DRY-O and O-TIP variables of high intensity (see Table 2), expressed for the most active compounds.

3.5 Molecular interaction fields of AChE active site

We have calculated molecular interaction fields (MIF's) defining the box that include the AChE active site gorge, and using the probes that mimic important structural elements of the ligands in the dataset. Those were: N1= probe which mimic protonated pyridinium nitrogen; N1: probe, resembles amino group of the linker, and the DRY probe mimicking aromatic moieties of inhibitors (tacrine and similar). Those structural elements are common to majority of inhibitors included in the set. The OC1 probe resembles the alkoxy substituents on the benzene ring of the compounds **68-79** and **97-110**. The fields obtained by N1= probe on the isocontour level of –8.0 kcal/mol are presented in Figure 5A. The important minima are located near backbone carbonyl group of His 440, hydroxyl group of Ser 200 side chain, and carboxyl group of the Glu 199 side chain. The former two residues belong to the catalytic triad, and the later one is also important for ACh hydrolysis, because it stabilizes the transition state in Ser 200 acylation, *via* electrostatic interactions with imidazole ring of the His 440. These results are also in accordance with the assumption that protonated nitrogen of the tacrine interacts with the backbone carbonyl of His 440, emphasizing the importance of such protonation for the AChE inhibition potency. The average distance between backbone carbonyl O of the His 440 and centroid defined on aromatic ring of the Trp 279 is 16.50-17.50 Å in various AChE crystal structures [60]. This distance corresponds to DRY-O variables 437-439 (in all three models), which are expressed for the majority of more

22

potent compounds, and usually connect MIFs' associated with pyridinium nitrogen and distal aromatic ring of tacrine comprising compounds (**68-110**). The DRY field on isocontour level of −2.0 kcal/mol is shown in Figure 5B. Three important minima are found, located between Trp 279 and Tyr 70 (PAS), and between Trp 84 and Phe 330 (AS). The third important minimum is found near Trp 432. Location of the DRY probe fields is in accordance with the well-known experimental and theoretical results about binding of dual inhibitors to AChE.

The fields of the N1: probe are found near hydroxyl group of Ser 286, located at the rim of active site gorge, on the opposite side of typical PAS residues. Relatively large minimum of the same probe is found near backbone carbonyl group of Trp 279; the side chain amino group of Asn 280; and the side chain carboxyl group of Glu 278. In AS site, N1: probe minima are found near backbone carbonyl group of Trp 84; as well as near side chain carbonyl (amido) group of Asn 85. Those fields are shown on Figure 5C on the isocontour level of −8.00 kcal/mol. Minima for OC1 probe are found near the backbone carbonyl group of Trp 279, the side chain amido group of Asn 280, and near hydroxyl group of Ser 286 side chain (Figure 5D). Closer visual inspection of docking solutions for **68-80** and **97-110**, showed that amino groups of the linker and alkoxy groups on the benzene ring are not close to any of the amino acid residues found by GRID, as possible sites of interactions with N1: and OC1 probe. In this case we couldn't relate docked conformations of the compounds and calculated MIF's for those two probes.

Please put the Figure 5 here

4. Predictivity of the models

Internal predictivity of the models was tested by cross-validation methods (LOO, LTO and RG). However, q^2 is by some authors considered as necessary, but not sufficient method to test the

23

predictivity of QSAR models [62]. Therefore, we randomly divided the original set on the training (78 compounds, designated as 'reduced training set') and test set (32 compounds, designated as 'test set 1'), to estimate the r^2 predictive value. This was done for all three types of conformations, OMEGA, ROCS and VINA. Compounds which belong to the test set 1, were marked by asterisk in Table 1. PLS statistics for the models derived from the reduced training set (for OMEGA, ROCS, and VINA conformations), did not differ significantly from the original set, that includes 110 compounds (See Table S10, Supplementary material). Moreover, models obtained included all important variables from the original models, as described above. The r^2 predictive values and standard error of prediction (SDEP) for the test set 1, are shown in Table 4 (the first three entries). Experimental vs. predicted values are given in Table S11 (Supplementary material) and in Figure 6. As with the original set, the model derived from ROCS conformations had superior predictive ability, comparing to models derived from OMEGA minimum, and the VINA docked conformations, with $r^2 = 0.834$ (3LV). In all test sets, predicted pIC_{50} values, for majority of the compounds, were within the log unit comparing with experimental values. In OMEGA test set, some compounds appeared as outliers, namely **15**, **107** (underestimated pIC_{50}), and **65**, **84** (overestimated pIC_{50}). Compounds **15** and **107** were in bent conformations, so the important long variables of high intensity (O-O 158, DRY-O 477 and O-N1 768) were not expressed for those compounds. This can be considered as the main reason for the lack of predictivity for those compounds. In ROCS test set, predicted pIC_{50} for both of these compounds (now present in extended conformations), fall within the range of one log unit from the experimental ones. Compound **65** was outlier in all three test sets. So far, we cannot offer explanation for this. Larger differences among r^2_{pred} values exist, comparing to q^2 (RG). This can be seen from r^2_{pred} values derived from test set 1, based on OMEGA, ROCS and VINA conformations of the compounds

24

(0.752, 0.834, and 0.679, respectively) and q^2 (RG) derived from the original set (0.64, 0.75, and 0.65). The r^2_{pred} is more sensitive on conformations used.

The division of set on the training and test set usually gives satisfactory predictive statistics, since it is often the case that compounds present in test set are congeners, or structurally very similar to the compounds in the training set. What we examined next, is weather the models derived are predictive for the structurally dissimilar compounds, and for compounds for which pIC_{50} values were determined on the different enzyme source (human AChE). Similar investigation was done by Bernard *et al.* [63]. They used the training set of 82 *N*-benzylpiperidine derivatives, whose inhibitory data were determined on mouse AChE, and test set of 29 *N*-benzylpiperidines with inhibitory data tested on human AChE. Good predictivity was achieved, demonstrating the ability of the model to predict the potency of the compounds tested on the different enzyme source, and in slightly different assay conditions (pH, temperature).

For the test set 2, we collected totally 40 compounds, comprising: 2,4-disupstituted pyrimidines (**111-119**, structurally dissimilar and tested on *Hu*AChE), dual tacrine inhibitors (**121-123**, structurally similar, but tested on *Hu*AChE), piperidine derivatives (**124-134**, structurally dissimilar and tested on *Ee*AChE), indanone derivatives (**135-145**, structurally dissimilar and tested on *Ee*AChE) and tacrine-ferulic acid dimers (**145-150**, structurally similar and tested on *Ee*AChE), Scheme 3. The original models (OMEGA, ROCS and VINA) derived from 110 compounds, were used for the prediction. Statistics for the external predicitivity (r^2_{pred} and SDEP) is given in Table 4 (the last three entries), experimental *vs.* calculated pIC_{50} values are given in Table S12 (Supplementary material) and in Figure 6. It is obvious that r^2_{pred} is highly sensitive on conformations used. It changes from poor, 0.469 (OMEGA model) to satisfactory predictivity of 0.740 (for VINA model). Potencies of the some of 2,4-disupstituted pyrimidines were less well

25

predicted in OMEGA and ROCS test set 2. These compounds are significantly smaller than compounds in the training set. Probably that those compounds even do not bind to both AS and PAS of AChE simultaneously, and therefore produce less hydrophobic contacts with aminoacid residues inside AChE active site gorge. Individual contributions from many short variables expressed for those compounds, give rise to the overestimation of their predicted pIC_{50} values. Surprisingly, pIC_{50} for compounds **148** and **149** (OMEGA and ROCS test set 2, respectively), were also less well predicted, although compounds are similar to tacrine-benzene dimers (**68-79** and **97-110**) and tested on *Ee*AChE, without the need for IC_{50} renormalization. For the conformations used for those compounds (bent conformation in OMEGA test set 2), long variables having high intensities in the model were not expressed, causing the underestimation of their pIC_{50} values. For piperidine derivatives **133** and **134**, OMEGA and ROCS model overestimated pIC_{50} values. Potencies of those compounds are fairly well predicted in VINA test set 2. The only outlier in VINA test set 2 was compound **135** (but fairly well predicted in OMEGA and ROCS test set 2); so far we could not offer explanation for this.

Both methods for the estimation of predictivity (division on training and test sets, and employment of truly external, and structurally dissimilar test set) gave good predictive statistics, expressed as r^2_{pred} (0.834 for ROCS test set 1 and 0.740 for VINA test set 2), considering large structural diversity of compounds in training and test sets. VINA model was highly successful in predicting potencies for compounds belonging to test set 2, structurally very dissimilar from the training set, and tested on the different enzyme source. Interestingly, predictivity of the original model derived from 110 compounds, was not sensitive on conformations used (similar q^2 values for OMEGA, ROCS, and VINA models), while predictivity of the external test set 2 was highly influenced by the conformations used (large discrepancy between r^2 of OMEGA, ROCS and

26

VINA, for the test set 2). The test set 2 was best predicted by VINA model, emphasizing the importance of using conformations built in reference to geometrical restrictions of AChE active site gorge.

Please put the Scheme 3 here

Please put the Table 4 here

Please put the Figure 6 here

5. Models based on 2D descriptors

Because it seemed that all three models, regardless on conformation used, contained the similar chemical information about structure-activity of AChE dual reversible inhibitors (although predictivity of the models was sensitive on conformations used), we have built model based on descriptors derived from the 2D structures of the compounds. Following blocks of 2D-dependent descriptors [64] from E-Dragon software [65] were considered: constitutional, functional group counts, topological, geometrical, atom centred fragments, and molecular properties. Descriptors were visually inspected and those having low or no variance manually excluded. The rest of descriptors, along with activity of compounds were imported in BILIN program [66], and systematic search up to four variables was performed. Model having the best statistics, obtained for the initial set of 110 compounds is given in Equation 1. Model built using the same descriptors for 150 compounds (training and test set 2) was still statistically valid, having something inferior statistics, Equation 2. Numerical values of descriptors for all compounds are given in Table S13. There is insignificant correlation between descriptors used, $r^2 < 0.1$.

27

$p(IC_{50}) = 0.716 (\pm 0.15)$ nR10 $+ 1.113 (\pm 0.25)$ N-070 $+ 5.446 (\pm 0.24)$ Equation 1

$(n = 110; r = 0.827; s = 0.697; F = 115.710; Q^2 = 0.656; s_{PRESS} = 0.728)$

$p(IC_{50}) = 0.653 (\pm 0.16)$ nR10 $+ 0.645 (\pm 0.27)$ N-070 $+ 5.736 (\pm 0.22)$ Equation 2

$(n = 150; r = 0.700; s = 0.862; F = 70.598; Q^2 = 0.465; s_{PRESS} = 0.883)$

n - number of objects, r - correlation coefficient, s - standard deviation, F - Fischer F test, Q^2 - leave one-out squared correlation coefficient, s_{PRESS} - standard deviation of the leave one-out cross-validated equation.

Both descriptors in correlations have a positive sign, so high potency of compounds is associated with increasing number of structural fragments described by the both of nR10 (number of 10-membered rings (from the pool of constitutional descriptors)) and N-070 (defined as number of Ar-NH-Al fragments (from the pool of the atom-centered fragments)). Visual inspection of the numerical values of descriptors given in Table S13 (Supplementary material) show that subsets having high potency (tacrine-multialkoxy benzenes and tacrine-xanomelines) indeed comprise both types of fragments, but both structural elements are ascribed to tacrine moiety alone (see Scheme S14, Supplementary material). For the homodimeric quinazolinimines and heterodimers of quinazolinimine and lipoic acid, only nR10 descriptor have a constant value of 2, but those compounds lack the N-070 fragment, due to double bond between central ring of the quinazoline moiety and the =N– connected to it. Bis-pyridinum compounds, or *N*-benzylpiperidine derivatives do not comprise condensed rings, or comprise just one moiety with condensed six-membered rings, and those compounds generally exert lower potency.

Despite fair statistics, predicted pIC_{50} values (Table S13 in Supplementary material) clearly show that the both models classify compounds according to the structural classes, as described above, but cannot distinguished molecules by their potencies within each class.

28

6. Conclusions

The 3D-QSAR analysis based on alignment independent descriptors (GRIND-2) was performed on the set of 110 structurally diverse AChE reversible inhibitors. We can conclude that for three sets of conformations used, all models derived had good statistics and predictivity. The most important variables, having the high impact, were expressed in all three models. The presence of HBA and HBD groups, at specific, relatively large distances is revealed as highly significant for the potency. Those groups are: protonated pyridinium nitrogen in the AS, amino groups of the linker, and the presence of electron-rich (alkoxy) substituents in moieties that most probably interact with PAS. However, the method failed to recognize specific structural elements favourable for binding to either the AS or the PAS of the AChE. Variables that can be constrained to either of those two regions were expressed usually for all compounds, and are related to different structural elements, even within the same subsets of the compounds and had different pattern of expression in the models. Therefore, the short variables were less informative in explaining SAR of the dataset used. MIF's calculated for the AChE using the N1= (pyridinium nitrogen) and DRY probes enabled us to relate long DRY-O variables with aminoacid residues belonging to catalytic triad (His 440) and PAS (Trp279 and Tyr 70), that are important for the ligand binding.

Predictivity of the models was tested by the division of the original set on the training and test set, and also by the external test set comprising 40 molecules (test set 2), structurally dissimilar comparing to initial 110 AChE inhibitors. Some of those compounds were tested on different enzyme source (*Hu*AChE). Predictivity of the models for the test set 2 was highly dependent upon conformation used. Model based on VINA docked conformations proved to be superior over other two models in predicting inhibition potency for the truly external test set (test set 2), reflecting the need for using conformations built according to geometrical restrictions of AChE active site gorge.

29

In analysis of the initial models, based on OMEGA, ROCS and VINA conformations, it seemed that all three models gave the same chemical information about favourable structural elements for AChE inhibition potency. But the predictivity of the external, structurally disimilar test set, emphasized the importance of the conformation of compounds used in the models.

The models based on 2D descriptors, derived for the sets comprising 110 compounds and 150 compounds, gave fair statistics, but both models only classified compounds according to the structural classes, and were not able to distinguish molecules by their potencies within each class.

So far published 3D QSAR studies of AChE reversible inhibitors [67], were mostly limited on CoMFA/CoMSIA (alignment dependent) models, derived from sets of compounds belonging to one class of AChE inhibitors (tetrahydroaminoacridines, *N*-benzylpiperidines and piperazines, carbamates, etc.). Usually such models, have very good statistics (r^2>0.9 and q^2>0.7), but can be applied for prediction of inhibition potency of only the narrow structural class of compounds. Our study emphasized the benefits of using the alignment independent descriptors. The set employed in this study was, so far, the most structurally diverse set of AChE reversible inhibitors used for 3D QSAR modelling. Chemical information condensed and enclosed by the models was proved comprehensive in potency predictions of another, structurally dissimilar, test set.

30

References:

[1] J. Hardy, D.J. Selkoe, The amyloid hypothesis of Alzheimer's disease: progress and problems on the road to therapeutics, Science 297 (2002) 353-356.

[2] L. Buée, T. Bussière, V. Buée-Scherrer, A. Delacourte, P.R. Hof, Tau protein isoforms, phosphorylation and role in neurodegenerative disorders, Brain Res. Rev. 33 (2000) 95-130.

[3] M. Tolnay, A. Probst, Tau protein pathology in Alzheimer's disease and related disorders, Neuropathol. Appl. Neurobiol. 25 (1999) 171-187.

[4] A.V. Terry Jr., J.J. Buccafusco, The cholinergic hypothesis of age and Alzheimer's disease-related cognitive deficits: recent challenges and their implications for novel drug development, J. Pharmacol. Exp. Ther. 306 (2003) 821-827.

[5] R.T. Bartus, On neurodegenerative diseases, models, and treatment strategies: lessons learned and lessons forgotten a generation following the cholinergic hypothesis, Exp. Neurol. 163 (2000) 495-529.

[6] P.J. Harrison, Pathogenesis of Alzheimer's disease - beyond the cholinergic hypothesis: discussion paper, J.R. Soc. Med. 79 (1986) 347-352.

[7] J. Varghese, J.P. Beck, M.J. Bienkowski, S. Sinha, R.L. Heinrikson, Human β-Secretase (BACE) and BACE Inhibitors, J. Med. Chem. 46 (2003) 4625-4630.

[8] D.J. Selkoe, Normal and abnormal biology of the beta-amyloid precursor protein, Annu. Rev. Neurosci. 17 (1994) 489-517.

[9] G. Gibney, S. Camp, M. Dionne, K. MacPhee-Quigley, P. Taylor, Mutagenesis of essential functional residues in acetylcholinesterase, Proc. Natl. Acad. Sci. U.S.A. 87 (1990) 7546-7550.

[10] A. Shafferman, B.Velan, A. Ordentlich, C. Kronman, H. Grosfeld, M. Leitner, Y. Flashner, S. Cohen, D. Barak, A. Naomi, Substrate inhibition of acetylcholinesterase: Residues affecting signal transduction from the surface to the catalytic center, EMBO J. 11 (1992) 3561-3568.

[11] Z. Radić, G. Gibney, S. Kawamoto, K. MacPhee-Quigley, C. Bongiorno, P. Taylor, Expression of recombinant acetylcholinesterase in a baculovirus system: kinetic properties of glutamate 199 mutants, Biochemistry, 31 (1992) 9760-9767.

[12] M. Ekholm, H. Konschin, Comparative model building of human butyrylcholinesterase, J. Mol. Struct. (Theochem) 467 (1990) 161-172.

[13] A. Ordentlich, D. Barak, C. Kronman, N. Ariel, Y. Segall, B. Velan, A. Shafferman, Functional characteristics of the oxyanion hole in human acetylcholinesterase, J. Biol. Chem. 273 (1998) 19509-19517.

[14] H. J. Kreienkamp, C. Weise, R. Raba, A. Aaviksar, F. Hucko, Anionic subsites of the catalytic center of acetylcholinesterase from Torpedo and from cobra venom, Proc. Natl. Acad. Sci.U.S.A. 88 (1991) 6117-6121.

[15] J. L. Sussman, M. Harel, F. Frolow, C. Oefner, A. Goldman, L. Toker, I. Silman, Atomic structure of acetylcholinesterase from Torpedo californica: a prototypic acetylcholine-binding protein, Science 253 (1991) 872-879.

[16] A. Ordentlich, D. Barak, C. Kronman, U. Flashner, M. Leitner, Y. Segall, N. Ariel, S. Cohen, B. Velan, A. Shafferman, Dissection of the human acetylcholinesterase active center determinants of substrate specificity. Identification of residues constituting the anionic site, the hydrophobic site, and the acyl pocket, J. Biol. Chem. 268 (1993) 17083-17095.

[17] D. C. Vellom, Z. Radić, L. Ying, N. A. Pickering, S. Camp, P. Taylor, Amino acid residues controlling acetylcholinesterase and butyrylcholinesterase specificity, Biochemistry 32 (1993) 12-17.

[18] P. Taylor, S. Lappi, Interaction of fluorescence probes with acetylcholinesterase. The site and specificity of propidium binding, Biochemistry 14 (1975) 1989-1997.

[19] D. Barak, C. Kronman, A. Ordentlich, A. Naomi, A. Bromberg, D. Marcus, A. Lazar, B. Velan, A. J. Shafferman, Acetylcholinesterase peripheral anionic site degeneracy conferred by amino acid arrays sharing a common core, J. Biol. Chem. 269 (1994) 6296-6305.

32

[20] Y. Bourne, P. Taylor, Z. Radić, P. Marchot, Structural insights into ligand interactions at the acetylcholinesterase peripheral anionic site, EMBO J. 22 (2003) 1-12.

[21] M. Bartolini, C. Bertucci, V. Cavrini, V. Andrisano, β-Amyloid aggregation induced by human acetylcholinesterase: inhibition studies, Biochem. Pharmacol. 65 (2003) 407-416.

[22] N. C. Inestrosa, A. Alvarez, A. C. Perez, R. D. Moreno, M. Vicente, C. Linker, O. I. Casanueva, C. Soto, Garrido, Acetylcholinesterase Accelerates Assembly of Amyloid-β-Peptides into Alzheimer's Fibrils: Possible Role of the Peripheral Site of the Enzyme, Neuron 16 (1996) 881-891.

[23] R. D. Cramer, D.E. Patterson, J. D. Bunce, Comparative molecular field analysis (CoMFA): I. Effect of shape on binding of steroids to carrier proteins, J. Am. Chem. Soc. 110 (1988) 5959–5967.

[24] W. Tong, E. R. Collantes, Y. Chen, W. J. Welsh, A comparative molecular field analysis study of *N*-Benzylpiperidines as acetylcholinesterase inhibitors, J. Med. Chem. 39 (1996) 380-387.

[25] K. K. Roy, A. Dixit, A. K. Saxena, An investigation of structurally diverse carbamates for acetylcholinesterase (AChE) inhibition using 3D-QSAR analysis, J. Mol. Graph. Mod. 27 (2008) 197-208.

[26] S. S. Chaudhaery, K. K. Roy, A. K. Saxena, Consensus superiority of the pharmacophore - based alignment, over maximum common substructure (MCS): 3D-QSAR studies on carbamates as acetylcholinesterase inhibitors J. Chem. Inf. Mod. 49 (2009) 1590-1601.

[27] Z. Haq, B. Wallenzohn, S. Tonmunphean, A. Khalid, M. I. Choudhary, B. B. Rode, 3D-QSAR Studies on natural acetylcholinesterase inhibitors of *Sarcococca saligna* by comparative molecular field analysis (CoMFA), Bioorg. Med. Chem. Lett. 13 (2003) 4375-4380.

[28] M. Recanatini, A. Cavalli, F. Belluti, L. Piazzi, A. Rampa, A. Bissi, S. Golli, P. Valenti, V. Andrisano, M. Bartolini, V. Cavrini, SAR of 9-Amino-1,2,3,4-tetrahydroacridine-based acetylcholinesterase inhibitors: synthesis, enzyme inhibitory activity, QSAR, and structure-based CoMFA of tacrine analogues, J. Med. Chem. 43 (2000) 2007-2018.

33

[29] N. Chen, L. Chunkai, L. Zhao, H. Zhang, 3D-QSAR study of multi-target-directed AChE inhibitors based on autodocking, Med. Chem. Res. 21 (2012) 245-256.

[30] L. Shen, G. Kiu, Y. Tang, Molecular docking and 3D-QSAR studies of 2-substituted 1-indanone derivatives as acetylcholinesterase inhibitors, Acta Pharmacol. Sin. 12 (2007) 2053-2063.

[31] Z. Ul-Haq, U. Mahmood, B. Jehangir, Ligand-based 3D-QSAR studies of physostigmine analogues as acetylcholinesterase inhibitors, Chem. Biol. Drug. Res. 74 (2009) 571-581.

[32] B.D. Silverman, D.E. Platt, M. Pitman, I. Rigoutsos, Comparative molecular moment analysis (CoMMA), in Kubinyi, H., Folkers, G. and Martin, Y.C. (Eds.) 3D QSAR in drug design: Vol. 3, Kluwer Academic Publishers, Dordrecht, The Netherlands, 1998, pp. 183–196.

[33] T.W. Heritage, A.M. Ferguson, D.B. Turner, P. Willett, EVA - a novel theoretical descriptor for QSAR studies, In Kubinyi, H., Folkers, G. and Martin, Y.C. (Eds.) 3D QSAR in drug design: Vol. 2, Kluwer Academic Publishers, Dordrecht, The Netherlands, (1998) 381–398.

[34] R. Todeschini, P. Gramatica, New 3D molecular descriptors: The WHIM theory and QSAR applications. In Kubinyi, H., Folkers, G. and Martin, Y.C. (Eds.) 3D QSAR in drug design: Vol. 2, Kluwer Academic Publishers, Dordrecht, The Netherlands, (1998) 355–380.

[35] A. Durán, I. Zamora, M. Pastor, Suitability of GRIND-based principal properties for the description of molecular similarity and ligand-based virtual screening, J Chem. Inf. Model. 49 (2009) 2129-2138.

[36] A. Samadi, M. Chioua, I. Bolea, C. Rios, J. Iriepa, J. Moraled, A. Bastida, G. Esteban, M. Unzeta, E. Galvez, J. Marco-Contelles, Synthesis, biological assessment and molecular modeling of new multipotent MAO and cholinesterase inhibitors as potential drugs for the treatment of Alzheimer's disease, Eur. J. Med. Chem, 46 (2011) 4665-4668.

[37] X. Chen, J. G. Tikhonova, M. Decker, Synthesis, biological assessment and molecular modeling of new multipotent MAO and cholinesterase inhibitors as potential drugs for the treatment of Alzheimer's disease, Bioorg. Med. Chem 19 (2011) 1222-1235.

34

[38] M. Decker, B. Kraus, J. Heilmann, Probing the mid-gorge of cholinesterases with spacer-modified bivalent quinazolinimines leads to highly potent and selective butyrylcholinesterase inhibitors, Biorg. Med. Chem. 16 (2008) 4252-4261.

[39] P. Kapkova, N. Stiefl, U. Surig, B. Engels, K. Baumann, U. Holzgrabe, Synthesis, biological activity, and docking studies of new acetylcholinesterase inhibitors of the bispyridinium type, Arch. Pharm. Pharm. Med. Chem. 336 (2003) 523-540.

[40] P. Kapkova, V. Alptuzun, P. Frey, E. Erciyas, U. Holzgrabe, Search for dual function inhibitors for Alzheimer's disease: Synthesis and biological activity of acetylcholinesterase inhibitors of pyridinium-type and their Ab fibril formation inhibition capacity, Biorg. Med. Chem. 14 (2006) 472-478.

[41] D. Silva, M. Chioua, A. Samadi, M. C. Carreiras, M. L. Jimeno, E. Mendes, C. Rios, A. Romero, M. Villaroya, M. G. Lopez, J. Marco-Contelles, Synthesis and pharmacological assessment of diversly substituted pyrazolo[3,4-*b*]quinolone, and benzo[*b*]pyrazolo[4,3-*g*][1,8]naphtyridine derivatives, Eur. J. Med. Chem, 46 (2011) 4676-4681.

[42] W. Luo, Y. Li, Y. He, S. Huang, D. Li, L. Gu, Z. Huang, Synthesis and evaluation of heterobivalent tacrine derivatives as potential multi-functional anti-Alzheimer agents, Eur. J. Med. Chem, 46 (2011) 2609-2616.

[43] W. Luo, Y. Li, Y. He, S. Huang, J. Tan, T. Ou, D. Li, L. Gu, Z. Huang, Design, synthesis and evaluation of novel tacrine-multialkoxybenzene hybrids as dual inhibitors for cholinesterases and amyloid beta aggregation, Bioorg. Med. Chem. 19 (2011) 763-770.

[44] L. Fang, S. Jumpertz, Y. Zhang, D. Apenroth, C. Fleck, K. Mohr, C. Trankle, M. Decker, Hybrid molecules from xanomeline and tacrine: Enhanced tacrine actions on cholinesterases and muscarinic M1 receptors, J. Med. Chem. 53 (2010) 2094-2103.

[45] L.G. Ellman, K.D. Courtney, V. Jr. Andres, M.R. Featherstone, A new and rapid colorimetric determination of acetylcholinesterase activity, Biochem. Pharmacol. 2 (1961) 88-90.

35

[46] S. Martin-Santamaria, J. Munoz-Muriedas, F. J. Luque, F. Gago, Modulation of binding strength in several classes of active site inhibitors of acetylcholinesterase studied by comparative binding energy analysis, J. Med. Chem. 47 (2004) 4471-4482.

[47] (a) J. Boström, Reproducing the conformations of protein bound ligands: A critical evaluation of several popular conformational tools, J. Comput. Aided Mol. Des. 15 (2002) 1137-1152; (b) J. Boström, J. R. Greenwood, J. Gottfries, Assessing the performance of OMEGA with respect to retrieving bioactive conformations, J. Mol. Graph. Model. 21 (2003) 449-462; OMEGA version 2.2.1, www.eyesopen.com.

[48] T. A. Halgren, MMFF VI. MMFF94s option for energy minimization studies, J. Comp. Chem. 20 (1999) 720-729.

[49] J. A. Grant, M. A. Gallardo, B. T. Pickup, A fast method of molecular shape comparison: A simple application of a Gaussian description of molecular shape, J. Comp. Chem. 17 (1996) 1653-1666; ROCS version 2.3.1, www.eyesopen.com.

[50] O. Trott, A. J. Olson, AutoDock Vina: improving the speed and accuracy of docking with a new scoring function, efficient optimization and multithreading, J. Comp. Chem. 31 (2010) 455-461; AutoDock Vina 1.0, http://vina.scripps.edu/

[51] A. Duran, G. C. Martinez, M. Pastor, Development and validation of AMANDA, a new algorithm for selecting highly relevant regions in Molecular Interaction Fields, J. Chem. Inf. Model. 48 (2008) 1813-1823; Pentacle 1.0.6, www.moldiscovery.com. (AMANDA)

[52] P. J. Goodford, A computational procedure for determining energetically favorable binding sites on biologically important macromolecules, J. Med. Chem. 28 (1985) 849-857; GRID 22c; http://www.moldiscovery.com.

[53] T. Mohamed, X. Zhao, L. K. Habib, J. Yang, P.P.N. Rao, design, synthesis and structure-activity relationship (SAR) studies of 2,4-disupstituted pyrimidine derivatives: dual activity as cholinesterase and Aβ-aggregation inhibitors, Bioorg. Med. Chem. 19 (2011) 2269-2281.

36

[54] S. Rizzo, A. Bisi, M. Bartolini, F. Mancini, F. Belluti, S. Gobbi, V. Andrisano, A. Rampa, Multi-target strategy to address Alzheimer's disease: design, synthesis and biological evaluation of new tacrine based dimers, Eur. J. Med. Chem. 46 (2011) 4336-4343.

[55] Y. E. Kwon, J. Y. Park, K. T. No, J. H. Shin, S. K. Lee, J. S. Eun, J. H. Yang, T. Y. Shin, D. K. Kim, B. S. Chae, J. Y. Leem, K. H. Kim, Synthesis, *in vitro* assay, and molecular modelling of new piperidine derivatives having dual inhibitory potency against acetylcholinesterase and $A\beta_{1-42}$ aggregation for Alzheimer's disease therapeutics, Bioor. Med. Chem. 15 (2007) 6596-6607.

[56] F. C. Meng, F. Mao, W. J. Shan, F. Qin, L. Huang, X. S. Li, Design, synthesis, and evaluation of indanone derivatives as acetylcholinesterase inhibitors and metal-chelating agents, Bioorg. Med. Chem. Lett. 22 (2012) 4462-4466.

[57] L. Fang, B. Kraus, J. Lehmann, J. Heilmann, Y. Zhang, M. Decker, Design, synthesis of tacrine-ferulic acid hybrids as multi-potent anti-Alzheimer drug candidates, Bioorg. Med. Chem. Lett. 18 (2008) 2905-2909.

[58] M. L. Bolognesi, A. Minarini, M. Rosini, V. Tumiatti, C. Melchiorre, From dual binding site acetylcholinesterase inhibitors to multi-target-directed ligands (MTDLs): A step forward in the treatment of alzheimer's Disease, Mini Rev. Med. Chem, 8 (2008) 960-967.

[59] Y.-P. Pang, P. Quiram, T. Jelacic, F. Hong, S. Brimijoin, Highly potent, selective, and low cost bis-tetrahydroaminacrine inhibitors of acetylcholinesterase. J. Biol. Chem. 271 (1996) 23646-23649.

[60] (a) M. Harel, I. Schalk, L. Ehret-Sabattier, F. Bouet, M. Goeldner, C. Hirth, P. Axelsen, I. Silman, J. L. Sussman, Quaternery ligand binding to aromatic residues in the active site gorge of acetylcholinesterase, Proc. Nat. Acad. Sci. USA, 90 (1993) 9031-9035; (b) E. H. Rydberg, B. Brunstein, H. M. Greenblatt, D. M. Wong, D. Shaya, L. D. Williams, P. R. Carlier, Y. Pang, I. Silman, J. L. Sussman, Complexes of alkylene-linked tacrine dimers with Torpedo californica Acetylcholinesterase: Binding of bis(5)-tacrine produces a dramatic rearrangement in the active-site gorge, J. Med. Chem. 49 (2006) 5491-5500.

[61] ADMET Predictor, version 6.0; Simulations Plus, Inc.; 2012; www.simulations-plus.com.

37

[62] A. Golbraikh, A. Tropsha, Beware of q^2!, J. Mol. Graph. Model. 20 (2002) 269-276.

[63] P. Bernard, D. B. Kireev, J. R. Chretien, P. L. Fortier, L. Coppet, Automated docking of 82 N-benzylpiperidine derivatives to mouse acetylcholinesterase and comparative molecular field analysis with 'natural' alignment, J. Comput. Aided Mol. Des. 13 (1999) 355-371.

[64] R. Todeschini, V. Consonni, (2000). Handbook of Molecular Descriptors. Wiley-VCH, Weinheim (Germany).

[65] I. V. Tetko, J. Gasteiger, R. Todeschini, A. Mauri, D. Livingstone, P. Ertl, V. A. Palyulin, E. V. Radchenko, N. S. Zefirov, A. S. Makarenko, V. Y. Tanchuk, V. V. Prokopenko, Virtual computational chemistry laboratory - design and description, *J. Comput. Aid. Mol. Des*. **19**, 2005, 453-463.

[66] H. Kubinyi, Quantitative Structure-Activity Relationships, 7. The bilinear model, a new model for nonlinear dependence of biological activity on hydrophobic character, J. Med. Chem. **20**, 1977, 625-629; http://www.kubinyi.de/bilin-program.html

[67] G. H. Lushington, J. X. Guo, M. M. Hurley, Acetylcholinesterase: molecular modeling with the whole toolkit, Curr. Top. Med. Chem. 6 (2006) 57-73.

Table 1 Experimental pIC_{50} for the compounds **1-110**

Comp. No.	pIC_{50}	Comp. No.	pIC_{50}	Comp. No.	pIC_{50}
1*	5.921	**38**	6.330	**75***	8.426
2*	6.567	**39**	5.031	**76**	8.506
3	7.796	**40***	5.455	**77**	8.417
4	7.584	**41**	5.848	**78**	8.812
5	5.398	**42***	5.846	**79**	8.932
6	7.886	**43**	5.863	**80***	8.016
7*	7.432	**44**	6.036	**81**	7.200
8	7.276	**45**	6.143	**82**	7.360
9	7.796	**46***	5.551	**83**	7.660
10	5.638	**47**	5.710	**84***	7.580
11	6.276	**48***	4.684	**85**	7.830
12*	6.267	**49***	4.943	**86***	7.870
13	6.480	**50**	4.932	**87**	7.970
14	6.692	**51**	6.236	**88**	7.990
15*	7.310	**52**	5.939	**89***	7.920
16	6.251	**53**	6.055	**90**	7.970
17	7.678	**54**	5.351	**91**	8.070
18	6.217	**55**	6.468	**92***	8.060
19*	6.752	**56**	5.762	**93**	8.180
20	7.745	**57**	5.684	**94**	7.640
21*	6.539	**58***	5.099	**95**	8.190
22	8.174	**59**	5.879	**96***	8.210
23	6.815	**60**	5.775	**97**	7.564
24	7.119	**61**	5.337	**98***	7.722
25	6.271	**62**	4.527	**99**	8.384
26*	5.976	**63**	5.842	**100***	8.352
27	6.207	**64**	4.996	**101**	8.714
28	6.101	**65***	4.588	**102**	8.346
29*	7.102	**66**	6.161	**103***	8.267
30	7.187	**67***	5.262	**104**	8.379
31	7.236	**68**	7.032	**105***	8.627
32	4.842	**69**	7.583	**106**	8.312
33*	5.547	**70**	8.194	**107***	8.127
34	5.339	**71***	7.971	**108**	8.236
35	5.358	**72***	8.728	**109**	8.562
36	6.129	**73**	8.947	**110**	8.217
37	5.712	**74**	8.939		

*Compounds included in the test set 1.

39

Table 2 Statistics for the PLS models derived, based on different conformations.

	LV	SSX	SSX$_{acc}$	SDEC	SDEP	R^2	R^2_{acc}	Q^2_{acc} (5RG)	Q^2_{acc} (LTO)	Q^2_{acc} (LOO)
OMEGA	1	34.73	34.73	0.77	0.80	0.60	0.60	0.57	0.60	0.58
	2	8.48	43.21	0.66	0.73	0.71	0.71	064	0.68	0.65
	3	13.62	56.83	0.63	0.73	0.03	0.73	0.64	0.66	0.65
ROCS	1	39.63	39.63	0.71	0.73	0.67	0.67	0.65	0.62	0.65
	2	7.78	47.40	0.56	0.62	0.12	0.79	0.74	0.69	0.75
	3	3.91	51.31	0.48	0.62	0.05	0.84	0.75	0.72	0.76
VINA	1	36.76	36.76	0.75	0.77	0.63	0.63	0.60	0.60	0.60
	2	7.69	44.45	0.63	0.70	0.11	0.74	0.67	0.68	0.68
	3	4.21	48.66	0.55	0.73	0.06	0.80	0.65	0.66	0.66

Abbreviations: SSX – X variable explanation, SDEC-Standard Deviation of Error of Calculation, SDEP-Standard Deviation of Error of Prediction. The 'acc' – states for cumulative value. Validation methods used for calculation of q^2 are: random groups (RG), leave two out (LTO), and leave one out (LOO).
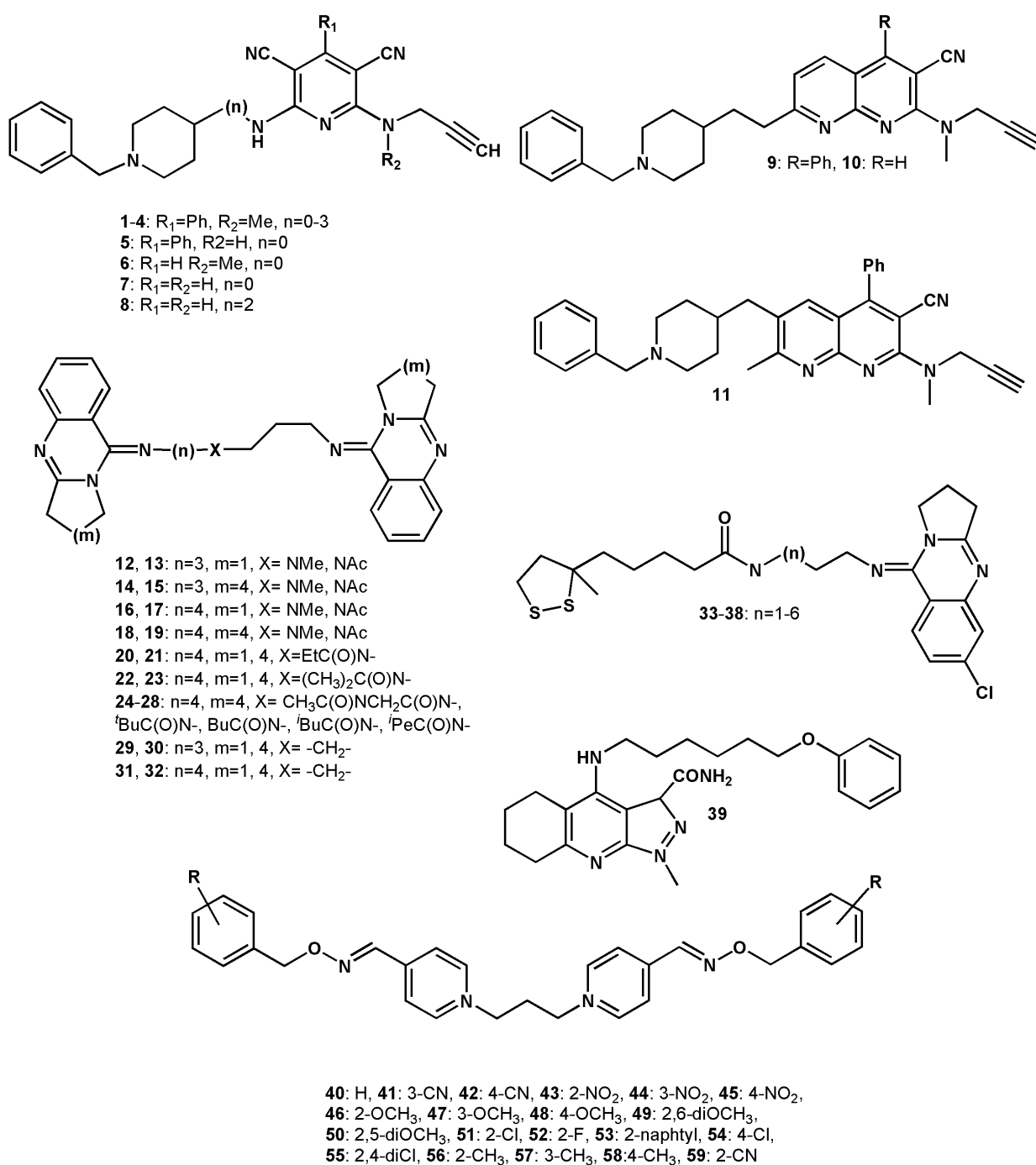
Table 3 The most important variables in the models based on different conformations

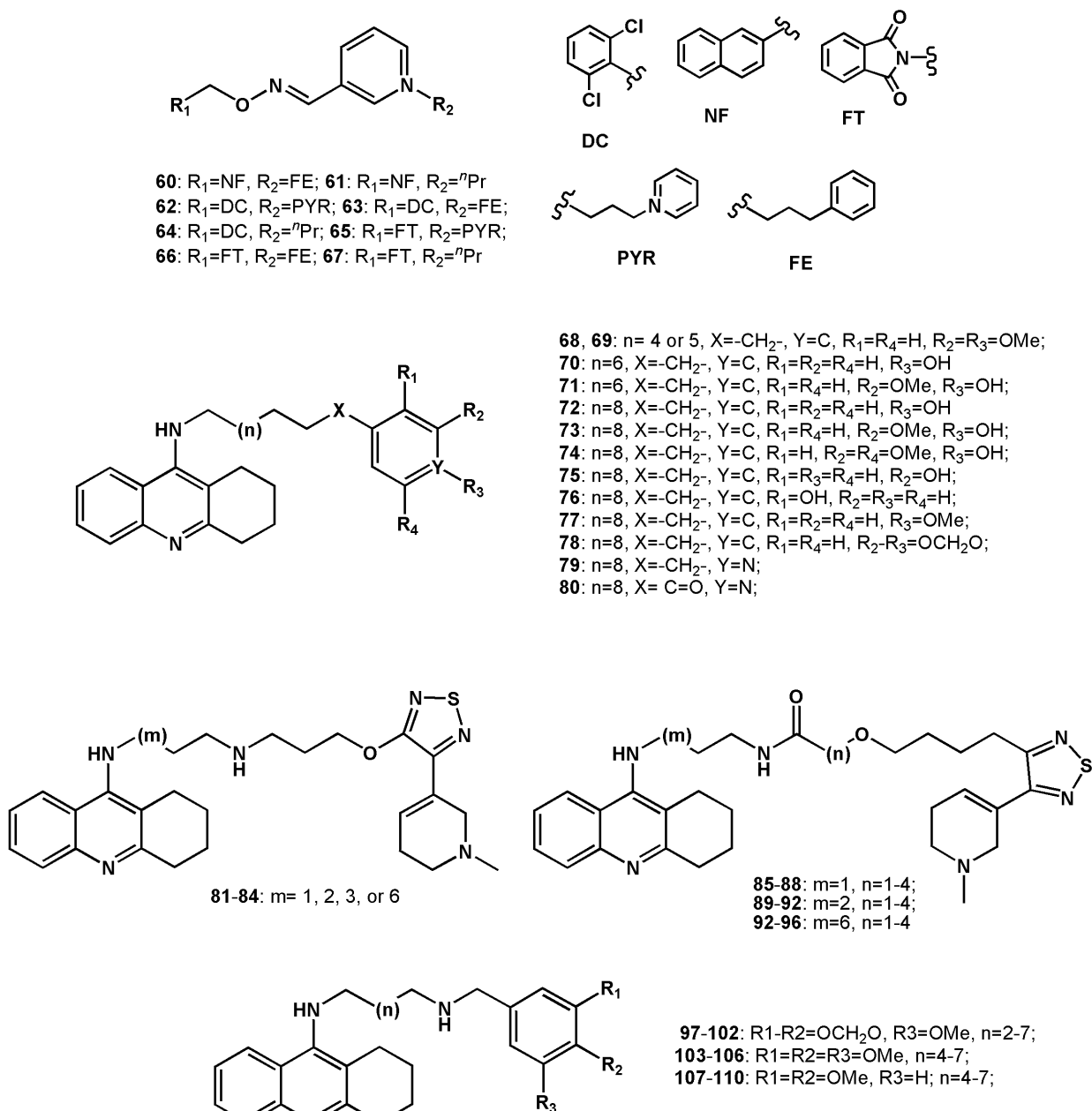| Block type	OMEGA	ROCS	VINA	Structural elements*	Expression
DRY-DRY	/	/	66 (31.12-21.44)	endmost benzene rings of bispyridinium compounds	Only for less potent
O-O	/	**128 (6.40-6.72)**	**114 (5.76-6.08)**	**miscellaneous**	**Highest negative impact. For majority.**
	147 (14.08-14.40)	144(11.52-11.84)	Low impact	dNH-Npyr or pNH-dNH	For the most active
	150-158 (16.96-17.92)	161 (19.96-17.28)	147 (16.32-16.64)	dNH-Npyr or pNH-dNH	For the most active
N1-N1	/	234 (5.76-6.08)	/	Binding to PAS	Most positive within the block. For majority
	263-268 (18.24-20.16)	278, 280 (19.84-20.80)	241 (15.68-16.00)	Oxime oxygens of bispyridinium dimmers	Only for less active compounds
DRY-O	455 (13.76-14.08)	475 (13.76-14.08)	427 (13.76-14.08)	Tac-dNH	For majority
	463 (16.32-16.64)	/	435 (16.32-16.64)	Tac-dNH	For majority
	477 (20.80-21.12)	496 (20.48-20.80)	444 (19.20-19.52)	Benzene-Npyr	Only for the most active
O-N1	745 (7.68-8.00) Positive impact	/	696-698 (7.68-8.64) Negative impact	dNH- Obenz in tacrine benzene dimers	For majority
	768 (15.04-15.36)	**805 (15.68-16.00)**	**723 (16.32-16.64)**	pNH-Obenz	**Highest positive impact** For majority
O-TIP	849 (8.00-8.32) Positive impact	888 (7.68-8.00) Positive impact	791 (7.36-7.68) Low negative impact	Npyr-tac, dNH-Obenz	For majority
	876 (16.64-16.96)	/	/	dNH-tac	For majority
	/	930 (21.12-21.44)	832 (20.48-20.80)	Npyr-endmost part	Only for the most active

40

*Explanations: tac – tacrine moiety; dNH-distal amino group of the linker, in respect to tacrine moiety; pNH-proximal amino group of the linker in respect to tacrine moiety, Npyr-pyridinium nitrogen, Obenz-alkoxy substituents on benzene ring.

Table 4. Predictive ability of the models (expressed as r^2_{pred} values) for the test set 1 (OMEGA, ROCS and VINA conformations); and the test set 2 (OMEGA, ROCS and VINA conformations) for the different dimensionalities of the models (number of LV's). The best values for r^2_{pred} and SDEP are given in bold.

		1 LV		2LV		3LV		4LV		5LV	
		r^2	SDEP	r^2	SDEP	r^2	SDEP	r^2	SDEP	r^2	SDEP
Test set 1	OMEGA	0.750	0.641	0.725	0.672	**0.752**	**0.638**	0.622	0.788	0.609	0.801
	ROCS	0.702	0.699	0.777	0.605	**0.834**	**0.522**	0.793	0.582	0.795	0.580
	VINA	0.627	0.782	**0.679**	**0.725**	0.657	0.750	0.619	0.790	0.515	0.892
Test set 2	OMEGA	0.360	0.803	0.397	0.779	0.423	0.762	0.314	0.814	**0.469**	**0.731**
	ROCS	0.452	0.739	**0.581**	**0.647**	0.460	0.734	0.482	0.719	0.533	0.683
	VINA	0.556	0.655	0.670	0.565	0.672	0.563	**0.740**	**0.501**	0.712	0.528

41

1-**4**: R$_1$=Ph, R$_2$=Me, n=0-3
5: R$_1$=Ph, R2=H, n=0
6: R$_1$=H R$_2$=Me, n=0
7: R$_1$=R$_2$=H, n=0
8: R$_1$=R$_2$=H, n=2

9: R=Ph, **10**: R=H

11

12, **13**: n=3, m=1, X= NMe, NAc
14, **15**: n=3, m=4, X= NMe, NAc
16, **17**: n=4, m=1, X= NMe, NAc
18, **19**: n=4, m=4, X= NMe, NAc
20, **21**: n=4, m=1, 4, X=EtC(O)N-
22, **23**: n=4, m=1, 4, X=(CH$_3$)$_2$C(O)N-
24-**28**: n=4, m=4, X= CH$_3$C(O)NCH$_2$C(O)N-,
^{t}BuC(O)N-, BuC(O)N-, ^{i}BuC(O)N-, ^{i}PeC(O)N-
29, **30**: n=3, m=1, 4, X= -CH$_2$-
31, **32**: n=4, m=1, 4, X= -CH$_2$-

33-**38**: n=1-6

39

40: H, **41**: 3-CN, **42**: 4-CN, **43**: 2-NO$_2$, **44**: 3-NO$_2$, **45**: 4-NO$_2$,
46: 2-OCH$_3$, **47**: 3-OCH$_3$, **48**: 4-OCH$_3$, **49**: 2,6-diOCH$_3$,
50: 2,5-diOCH$_3$, **51**: 2-Cl, **52**: 2-F, **53**: 2-naphtyl, **54**: 4-Cl,
55: 2,4-diCl, **56**: 2-CH$_3$, **57**: 3-CH$_3$, **58**:4-CH$_3$, **59**: 2-CN

Scheme 1 Structures of the compounds **1-59**, used as dataset

42

60: R$_1$=NF, R$_2$=FE; **61**: R$_1$=NF, R$_2$=^{n}Pr
62: R$_1$=DC, R$_2$=PYR; **63**: R$_1$=DC, R$_2$=FE;
64: R$_1$=DC, R$_2$=^{n}Pr; **65**: R$_1$=FT, R$_2$=PYR;
66: R$_1$=FT, R$_2$=FE; **67**: R$_1$=FT, R$_2$=^{n}Pr

DC

NF

FT

PYR

FE

68, **69**: n= 4 or 5, X=-CH$_2$-, Y=C, R$_1$=R$_4$=H, R$_2$=R$_3$=OMe;
70: n=6, X=-CH$_2$-, Y=C, R$_1$=R$_2$=R$_4$=H, R$_3$=OH
71: n=6, X=-CH$_2$-, Y=C, R$_1$=R$_4$=H, R$_2$=OMe, R$_3$=OH;
72: n=8, X=-CH$_2$-, Y=C, R$_1$=R$_2$=R$_4$=H, R$_3$=OH
73: n=8, X=-CH$_2$-, Y=C, R$_1$=R$_4$=H, R$_2$=OMe, R$_3$=OH;
74: n=8, X=-CH$_2$-, Y=C, R$_1$=H, R$_2$=R$_4$=OMe, R$_3$=OH;
75: n=8, X=-CH$_2$-, Y=C, R$_1$=R$_3$=R$_4$=H, R$_2$=OH;
76: n=8, X=-CH$_2$-, Y=C, R$_1$=OH, R$_2$=R$_3$=R$_4$=H;
77: n=8, X=-CH$_2$-, Y=C, R$_1$=R$_2$=R$_4$=H, R$_3$=OMe;
78: n=8, X=-CH$_2$-, Y=C, R$_1$=R$_4$=H, R$_2$-R$_3$=OCH$_2$O;
79: n=8, X=-CH$_2$-, Y=N;
80: n=8, X= C=O, Y=N;

81-**84**: m= 1, 2, 3, or 6

85-**88**: m=1, n=1-4;
89-**92**: m=2, n=1-4;
92-**96**: m=6, n=1-4

97-**102**: R1-R2=OCH$_2$O, R3=OMe, n=2-7;
103-**106**: R1=R2=R3=OMe, n=4-7;
107-**110**: R1=R2=OMe, R3=H; n=4-7;

Scheme 2 Structures of the compounds **60-110**, used as dataset

43

R_2 = **111,115**: pyrolidine
112,116: morpholine
113,118: tiomorpholine
114,119: 4-methylpiperidine
115: N-acetylpiperazine

111-**115**

116-**119**

120: n=7, R=H, R1=**A**
121: n=7, R=Cl, R1=**B**
122: n=7, R=Cl, R1=**C**

121-**122**

A

B

C

D

123

124-**132**: R=benzhydryl, R_1= **124**: H, **125**: 4-F,
126: 4-NO_2, **127**: 4-tBu, **128**: 4-iPr, **129**: 3-Cl,
130: 3-F, X=NH, **131**: 4-Cl, X=NH, **132**: 4-F.
133,134: R=benzyl, R_1= 4-tBu or 4-iPr.

135-**139**: R_1=piperidine, n=3-6 and 9.
140: n=4, R_1=pyrolidine
141: n=4, R_1=diethylamine
142: n=6, R_1=imidazole

135-**142**

143-**145**: n=2,3 or 5

146-**150**: n=2-5 and 8

Scheme 3 Structures of the compounds **111-150**, used as test set 2

44

Figure captions

Scheme 1 Structures of the compounds **1**-**59** used as dataset

Scheme 2 Structures of the compounds **60**-**110** used as dataset
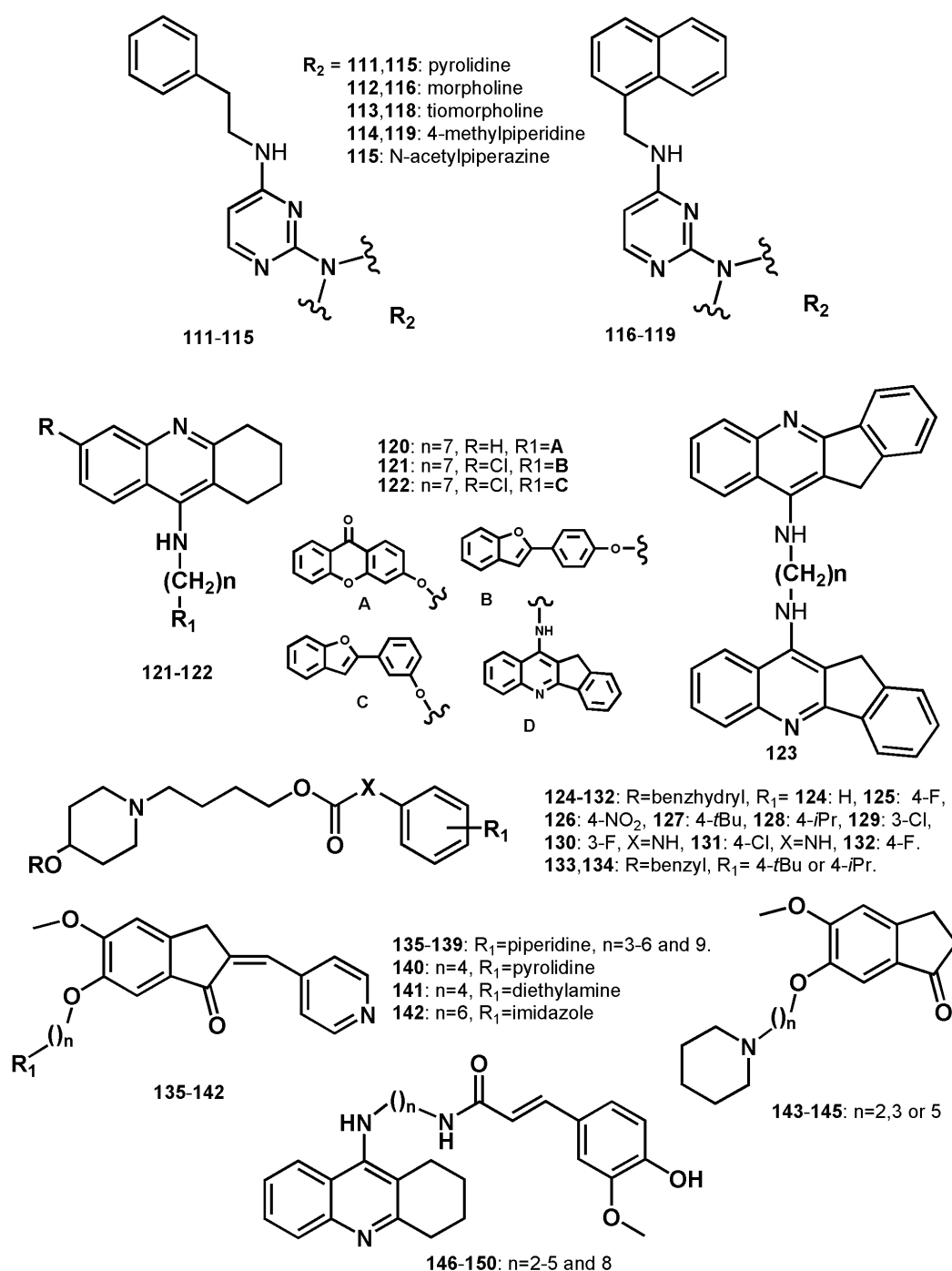
Scheme 3 Structures of the compounds **111**-**150**, used as test set 2

Figure 1 PLS coefficients plots (3LV) for the obtained models, based on: (a) OMEGA minimum energy conformations, (b) ROCS conformations, (c) docked conformations. The type of variable blocks are indicated by color: yellow, DRY-DRY; red, O-O; blue, N1-N1; green, TIP-TIP; cyan, DRY-O; magenta, DRY-N1; navy blue, DRY-TIP; dark green, O-N1; pink, O-TIP; grey, N1-TIP. Variables assigned by red coloured numbers are specific for the particular model.

Figure 2 The most important variables derived from model based on OMEGA minimum energy conformations: (a) O-O 158 (16.96-17.92 Å), (b) DRY-O 455 (13.76-14.08 Å), (c) DRY-O 477 (20.80-21.12 Å), (d) 745 O-N1 (7.68-8.00) (e) O-N1 768 (15.04-15.36 Å), (f) O-TIP 875 (16.32-16.64 Å).
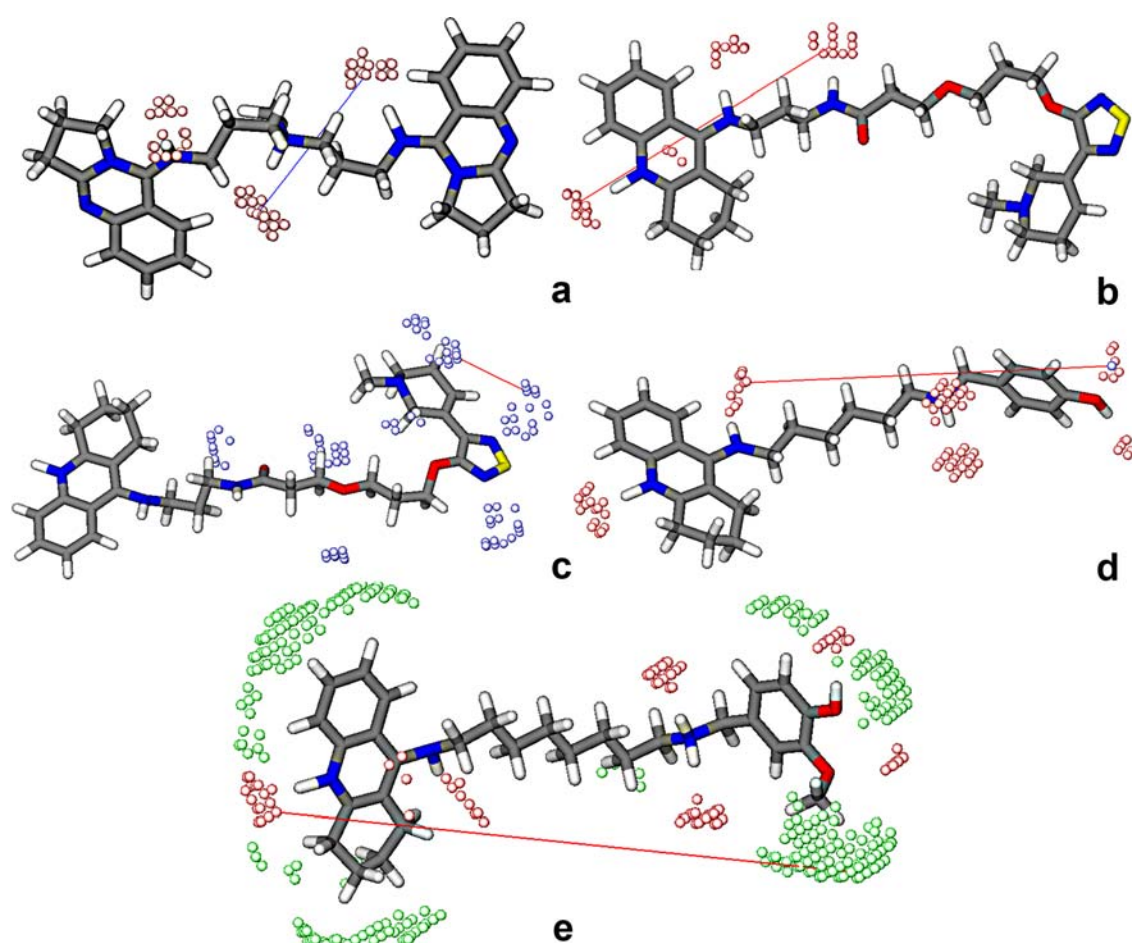
Figure 3 The most important variables derived from model based on the ROCS conformations: (a) O-O 128 (6.40-6.72 Å), (b) O-O 147 (12.48-12-80 Å), (c) N1-N1 234 (5.76-6.08 Å), (d) O-N1 805 (15.68-16.00 Å), (f) O-TIP 930 (21.12-21.44 Å).
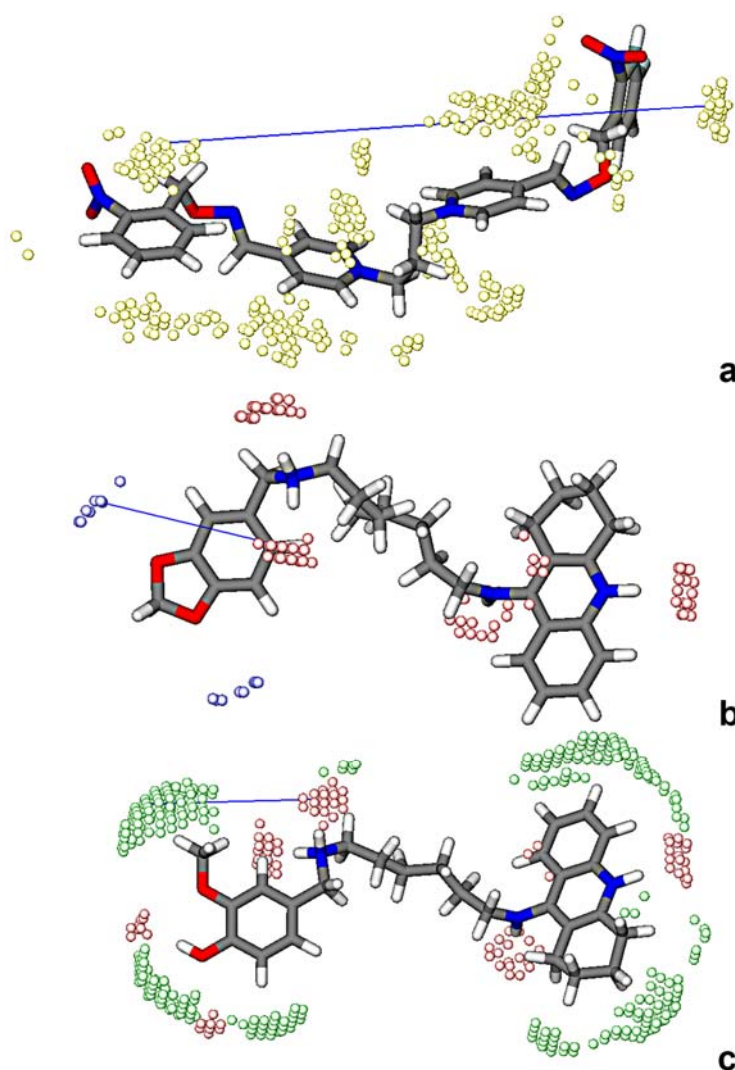
Figure 4 The most important variables derived from model based on VINA docked conformations: (a) DRY-DRY 66 (21.12-21.44 Å), (b) O-N1 697 (7.68-8.00 Å), (c) O-TIP 791 (7.36-7.68 Å)
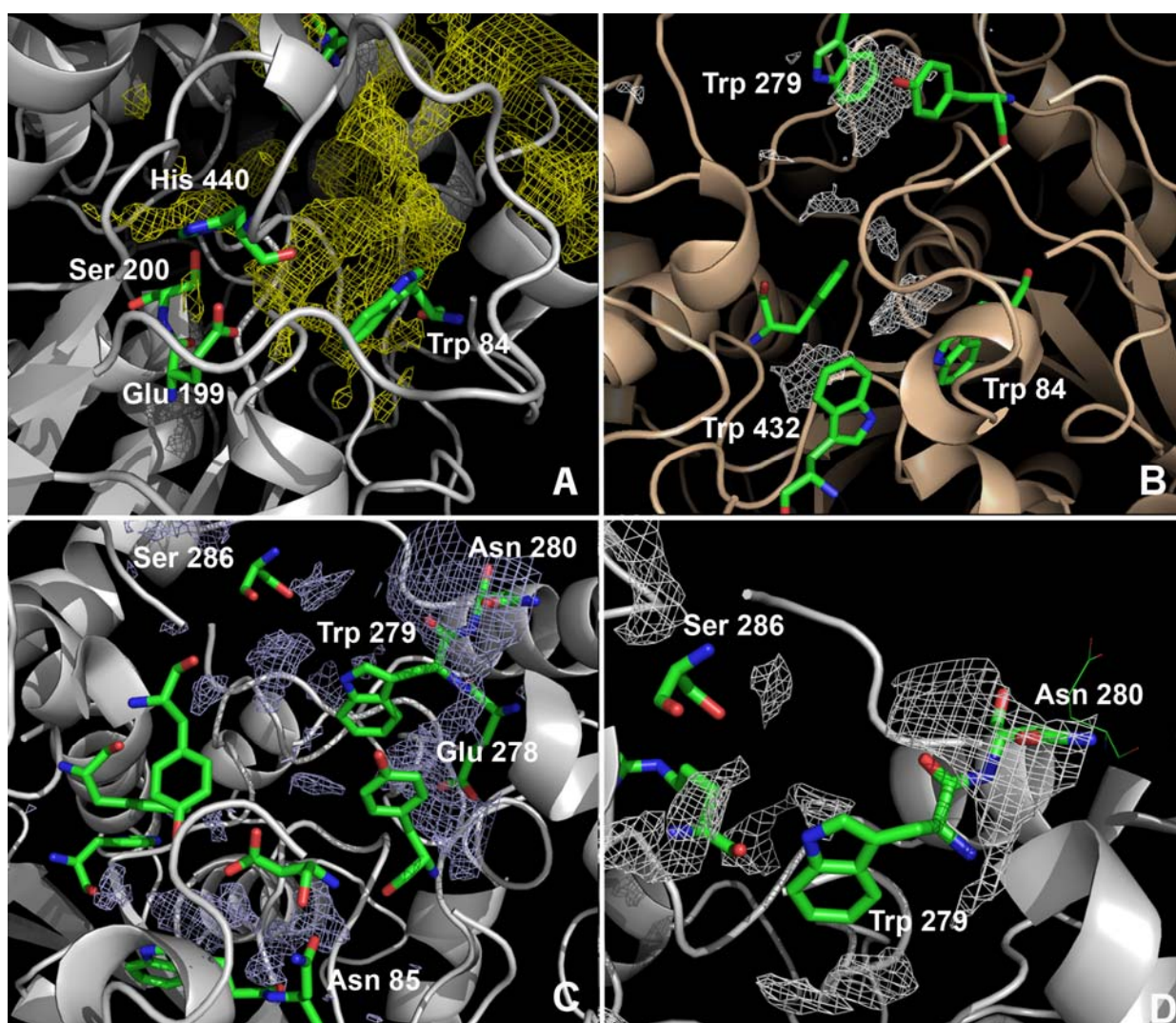
Figure 5 Calculated MIF's for AChE active site gorge: A. N1= probe, B. DRY probe, C. N1: probe, D. OC1 probe.
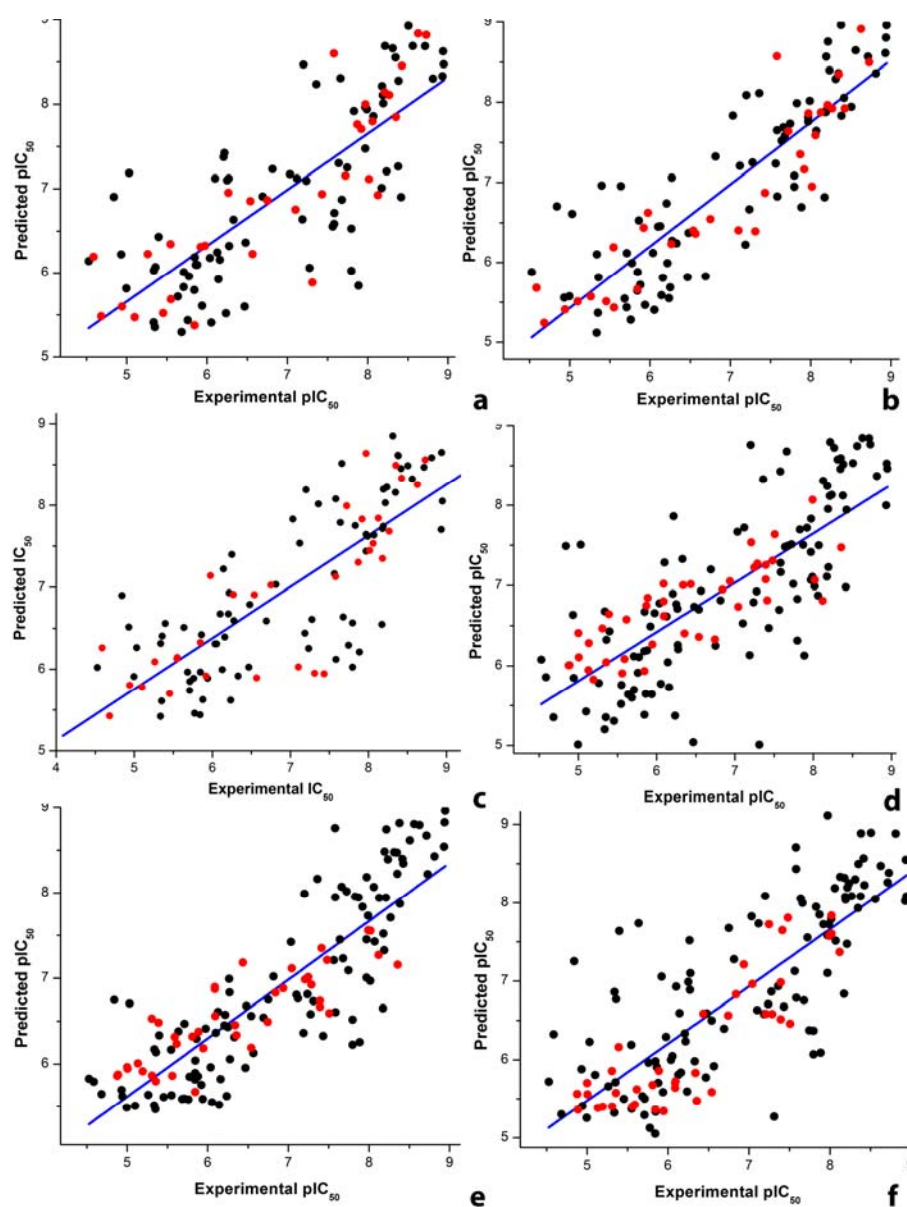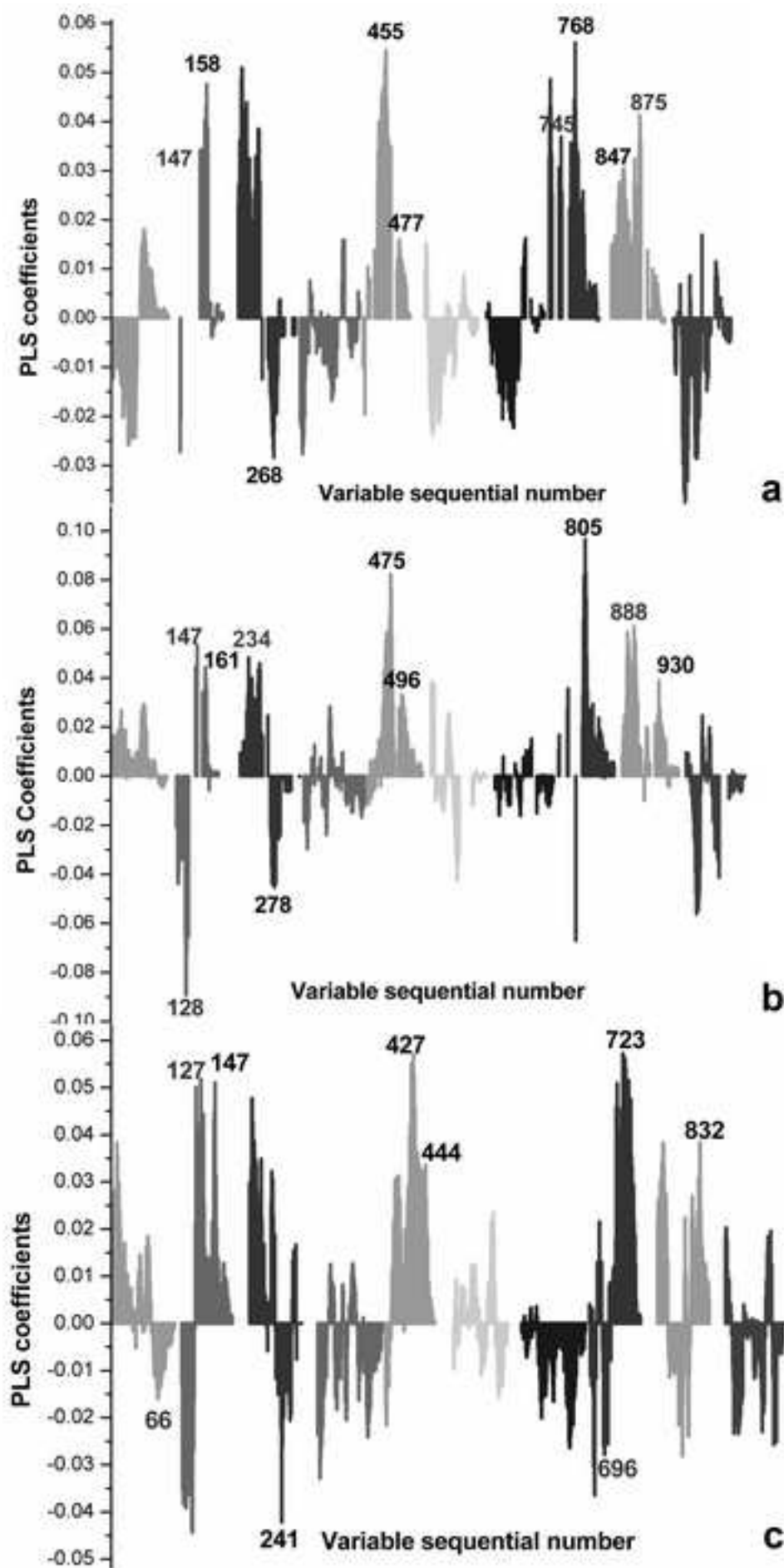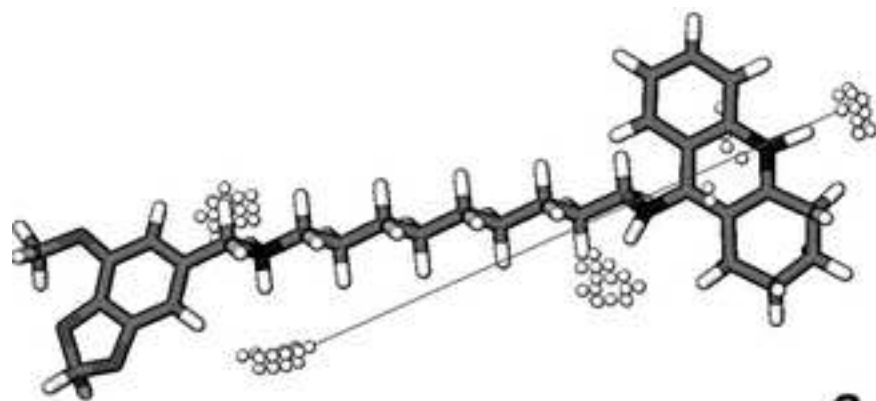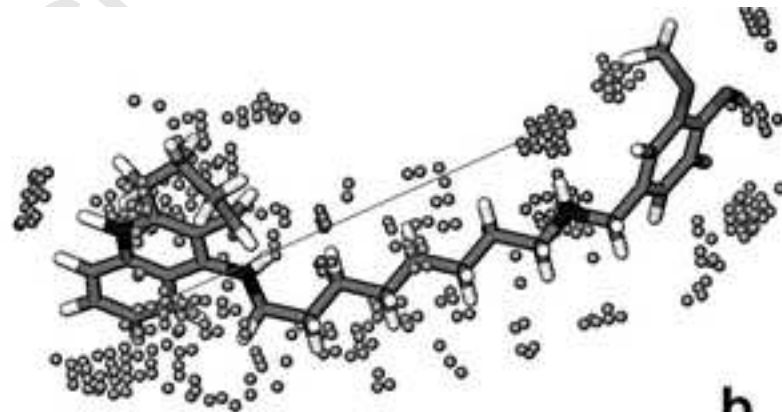
45

Figure 6. Experimental *vs*. predicted pIC_{50} values for test set 1 (a) OMEGA conformations, (b) ROCS conformations, (c) VINA conformations; and test set 2 (d) OMEGA conformations, (e) ROCS conformations, (f) VINA conformations.
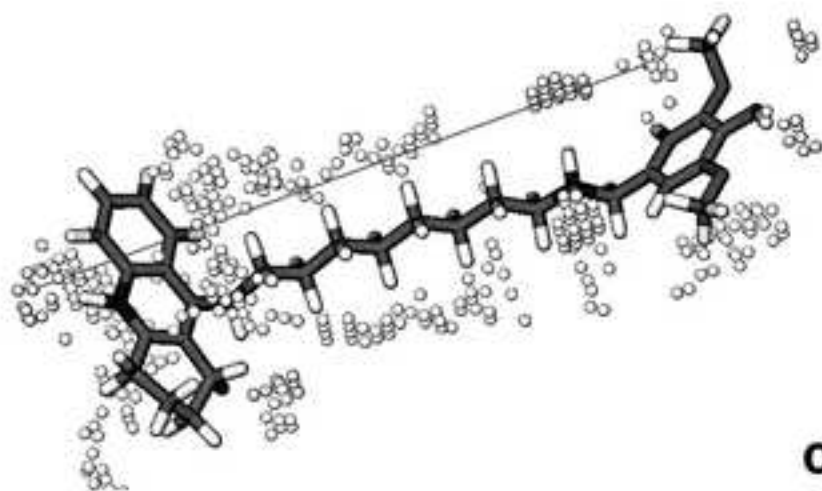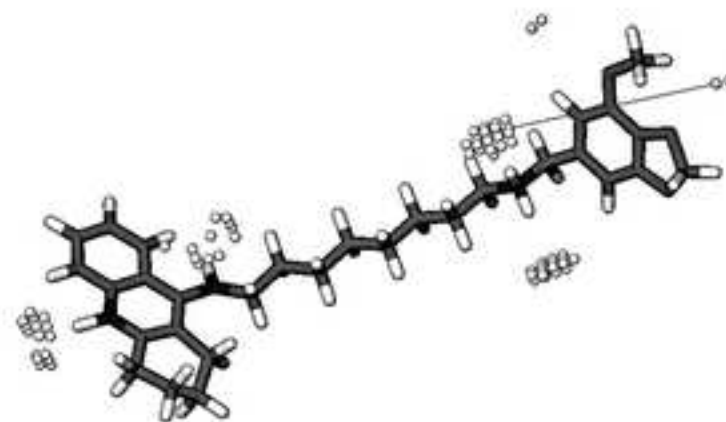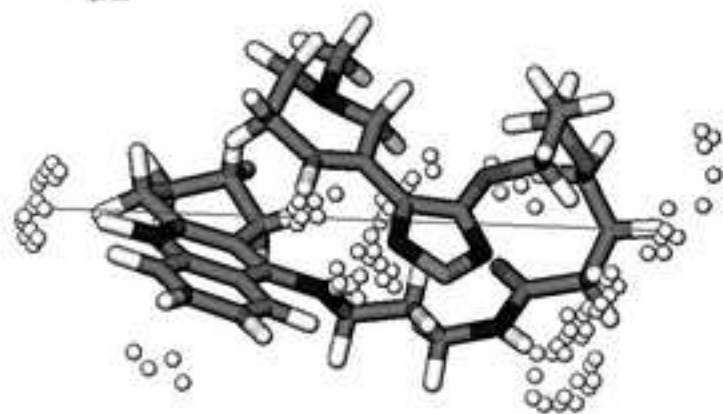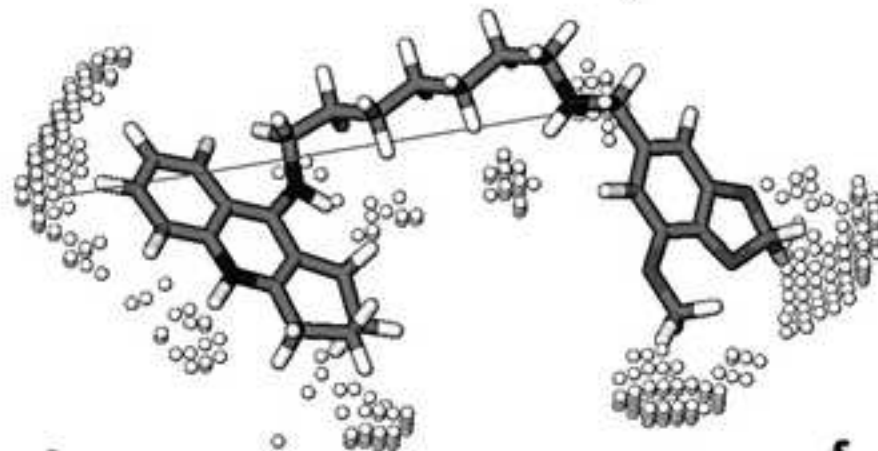
Figure 1 PLS coefficients plots (3LV) for the obtained models, based on: (a) OMEGA minimum energy conformations, (b) ROCS conformations, (c) VINA docked conformations. The type of

variable blocks are indicated by color: yellow, DRY-DRY; red, O-O; blue, N1-N1; green, TIP-TIP; cyan, DRY-O; magenta, DRY-N1; navy blue, DRY-TIP; dark green, O-N1; pink, O-TIP; grey, N1-TIP. Variables assigned by red coloured numbers are specific for the particular model.

Figure 2 The most important variables derived from model based on OMEGA minimum energy conformations: (a) O-O 158 (16.96-17.92 Å), (b) DRY-O 455 (13.76-14.08 Å), (c) DRY-O 477 (20.80-21.12 Å), (d) 745 O-N1 (7.68-8.00) (e) O-N1 768 (15.04-15.36 Å), (f) O-TIP 875 (16.32-16.64 Å).

49

Figure 3 The most important variables derived from model based on the ROCS conformations: (a) O-O 128 (6.40-6.72 Å), (b) O-O 147 (12.48-12-80 Å), (c) N1-N1 234 (5.76-6.08 Å), (d) O-N1 805 (15.68-16.00 Å), (f) O-TIP 930 (21.12-21.44 Å).

Figure 4 The most important variables derived from model based on VINA docked conformations:

(a) DRY-DRY 66 (21.12-21.44 Å), (b) O-N1 697 (7.68-8.00 Å), (c) O-TIP 791 (7.36-7.68 Å)

50

Figure 5. MIF's calculated for AChE active site gorge: A. N1= probe, B. DRY probe, C. N1: probe, D. OC1 probe.

Figure 6. Experimental *vs*. predicted pIC$_{50}$ values for test set 1 (a) OMEGA conformations, (b) ROCS conformations, (c) VINA conformations; and the test set 2 (d) OMEGA conformations, (e) ROCS conformations, (f) VINA conformations.

52